Petroleum Science 23 (2026) 5800–5818

Contents lists available at ScienceDirect

Petroleum Science

journal homepage: www.keaipublishing.com/en/journals/petroleum-science

Original Paper

Solubility and dissolution mechanism of novel multi-ester headgroup surfactants in supercritical CO_2

Ning Xu [a,b,c], Yan-Ling Wang [a,b,c,*], Baojun Bai [d], Shi-Zhang Cui [e], Yu Zhang [a,b,c], Wen-Jing Shi [a,b,c], Zhao-Nian Zhang [a,b,c], Wen-Hui Ding [a,b,c], Pei-Xu Ma [a,b,c], Zan Gao [a,b,c]

[a] Key Laboratory of Unconventional Oil & Gas Development (China University of Petroleum (East China)), Ministry of Education, Qingdao, 266580, Shandong, China
[b] School of Petroleum Engineering, China University of Petroleum (East China), Qingdao, 266580, Shandong, China
[c] Shandong Key Laboratory of Oil and Gas Field Chemistry, Qingdao, 266580, Shandong, China
[d] Geosciences and Geological and Petroleum Engineering, Missouri University of Science and Technology, Rolla, MO, 65409, United States
[e] Deshi Energy Technology Group Co. Ltd, Dongying, 257000, Shandong, China

ARTICLE INFO

Article history:
Received 27 October 2025
Received in revised form
4 June 2026
Accepted 5 June 2026
Available online 11 June 2026

Edited by Yan-Hua Sun

Keywords:
Supercritical CO_2 ($scCO_2$)
Surfactant
Solubility
Ester group
Interaction
Conformation

ABSTRACT

To address the limited solubility and applicability of conventional hydrocarbon surfactants in supercritical CO_2, a series of multi-ester headgroup surfactants were designed and synthesized by leveraging the CO_2-philic properties of ester groups. The molecular structures were characterized using Fourier transform infrared (FT-IR) spectroscopy and ^1H NMR. A custom-designed laser-based apparatus was developed to quantify surfactant solubility and systematically investigate phase behavior in CO_2. Molecular dynamics (MD) simulations were employed to elucidate structure–solubility relationships across multiple scales, including solubility parameters, interaction energies, radial distribution functions (RDFs), and free volume fractions. Results indicate that, at 323.15 K, the cloud-point pressure of a 1 wt% multi-ester headgroup surfactant in CO_2 is below 12 MPa. This value is substantially lower than the typical minimum miscibility pressure (MMP) between crude oil and CO_2 in Chinese reservoirs. The number and arrangement of ester groups synergistically affect solubility, with linear configurations outperforming cyclic ones and an optimal ester count ($n = 5$) maximizing solubility. Surfactant–CO_2 interactions are primarily governed by van der Waals and electrostatic forces, with van der Waals contributions exceeding 70%. RDF analysis reveals that carbonyl oxygen (O1) and terminal methyl carbon (C1) in the ester group are the primary CO_2 binding sites, enhancing CO_2-philicity via Lewis acid–base (LA–LB) and dispersion interactions. Linear ester side chains exhibit enhanced flexibility and conformational adaptability. The free volume fraction initially increases and then decreases with increasing ester group count, with the optimal configuration (MEG-L5) showing maximal chain extension and CO_2 contact efficiency during dissolution. Given that hydrocarbon surfactants primarily interact with CO_2 through LA–LB and dispersion forces, the design focus is on optimizing the density and arrangement of CO_2-philic segments. This modulates entropy changes to enhance favorable enthalpic interactions. This study elucidates the dissolution mechanisms of multi-ester headgroup surfactants in supercritical CO_2 ($scCO_2$) and identifies the molecular factors controlling their CO_2-philicity. These insights provide a theoretical basis for designing green, fluorine-free, cost-effective CO_2-philic surfactants for enhanced oil recovery.

1. Introduction

Low-permeability reservoir development has undergone rapid global expansion. By 2023, production from these reservoirs reached 2.24×10^8 t of oil equivalent, representing 27.19% of global oil production (Dai et al., 2024). Supercritical CO_2, with its low density and

* Corresponding author.
E-mail address: wangyl@upc.edu.cn (Y.-L. Wang).
Peer review under the responsibility of China University of Petroleum (Beijing).

https://doi.org/10.1016/j.petsci.2026.06.010

viscosity, enables effective injection into tight reservoirs. CO_2-based enhanced oil recovery (CO_2-EOR) is a highly economical technology within carbon capture, utilization, and storage (CCUS) frameworks (Zhang et al., 2020). Among CO_2-EOR methods, miscible CO_2 flooding provides the greatest potential for enhancing oil recovery. However, the minimum miscible pressure (MMP) for Chinese continental crude oils is typically elevated due to abundant heavy hydrocarbon fractions. Drawing on conventional hydrophilic–lipophilic surfactants, which significantly reduce oil–water interfacial tension at low concentrations (Alvarez and Schechter, 2017; Sukee et al., 2022a, 2022b; Standnes et al., 2002; Xie et al., 2005), Hoefling et al. (1991) proposed the concept of CO_2-philic–oleophilic surfactants. Adding these surfactants is a critical strategy for reducing MMP and enhancing CO_2–crude oil miscibility. However, due to the weak polarity of CO_2 and low solvent strength, only a few surfactants exhibit adequate solubility in CO_2. Thus, developing surfactants with high CO_2 solubility is an urgent priority.

DeSimone et al. (1992) first synthesized 1,1-dihydroperfluorooctyl acrylate (FOA) in supercritical CO_2, showing that specific functional groups can enhance surfactant CO_2-philicity. Subsequent studies confirmed the strong CO_2 affinity of fluorinated compounds (Dardin et al., 1998; Temtem et al., 2007; Yee et al., 1992). Similarly, siloxane-based surfactants show high CO_2 solubility due to flexible chains and elevated interfacial activity (Demirtas and Dilek, 2019; Lee et al., 2017; Shi and Qiao, 2017). However, environmental and cost concerns limit the industrial application of fluorinated and siloxane surfactants. Consequently, green, cost-effective hydrocarbon-based CO_2-philic surfactants have gained significant attention. Studies have shown that oxygen-containing groups, including carbonyls (Altarsha et al., 2012), esters (Liao et al., 2020), and ethers (Liu et al., 2001, 2002a, 2002b; Lv et al., 2020; Zhang et al., 2024a), primarily drive the CO_2-philicity of hydrocarbon surfactants. Kilic et al. (2007) quantified CO_2 affinity with ether, carbonyl, and ester groups using physical experiments and quantum chemical calculations. Although ether groups have higher single-point binding energy (−18.6 kJ/mol) than carbonyl or ester groups, esters offer three distinct binding modes, resulting in stronger overall interactions. This explains the higher CO_2 solubility of ester-containing polymers (e.g., PVAc) compared to ether-containing counterparts. The enhanced CO_2-philicity of ester groups stems from four key factors: (1) In addition to Lewis acid–base (LA–LB) interactions, a weak C–H···O hydrogen bond (0.5–1.0 kcal/mol) synergistically enhances CO_2–ester group interactions. LA–LB interactions between CO_2 and carbonyl groups are a key focus in designing CO_2-philic compounds (Kazarian et al., 1996). Furthermore, a weak C–H···O hydrogen bond between the ester group and CO_2, combined with LA–LB interactions, forms a primary–secondary interaction network that strengthens LA–LB interactions (Raveendran and Wallen, 2002). (2) Optimal ester group density primarily drives CO_2 solubility. Potluri et al. (2002) showed that fully acetylated monosaccharides dissolve in CO_2 at 5.17 MPa (298 K), with CO_2-philicity comparable to fluorinated materials. (3) Ester group spatial accessibility is critical for high solubility. Potluri et al. (2003) demonstrated via X-ray diffraction that outward-oriented, non-embedded acetoxy groups form dual-point CO_2 interactions, with orientation outweighing quantity as the determining factor. Ma et al. (2010) reported notable CO_2 affinity variations among sugar acetate isomers, identifying the influence order as: ester group accessibility > ester group number > molecular size. (4) Terminal group branching increases molecular free volume, thus enhancing CO_2 solubility (Bao et al., 2017). Bray et al. (2010) demonstrated that branched ester chains improve solubility by up to twentyfold, with an optimal acyl chain length of eight. Although these structural design principles enhance CO_2 solubility, the dominant mechanism remains unclear.

Molecular simulation is a critical tool for studying supercritical CO_2 systems (Criscenti and Cygan, 2013; Zhao et al., 2011, 2015), widely applied to phase equilibria and CO_2-EOR processes (Inomata et al., 1996; Liu et al., 2015). Early simulations focused on microscopic swelling and dissolution of CO_2 with hydrocarbons, such as CO_2–decane (Liu et al., 2015) and CO_2–octane (Zhang et al., 2013), elucidating intermolecular interaction mechanisms. Recently, research has shifted to CO_2–surfactant systems. Wang et al. (2016) reported that bent tail conformations of mixed surfactants (F_7H_n) enhance CO_2-philicity, while Gong et al. (2024) found that van der Waals forces dominate CO_2–polyether interactions, lowering CO_2–oil interaction energy. Zhang et al. (2024a) demonstrated that poly(propylene oxide) groups have greater CO_2-philicity than poly(ethylene oxide) groups, while Xu et al. (2025) showed that interaction energy and molecular conformation determine the CO_2 affinity of ethylene oxide segments. Zhang et al. (2024b) demonstrated that acetylating triisobutyl citrate hydroxyl groups increased CO_2 affinity and reduced MMP by 0.43 MPa, with acetylated C_6PO_3 showing a 13.77% lower MMP than its unmodified form. As surfactant solubility in CO_2 is essential for effective CO_2-EOR applications, understanding their dissolution behavior holds significant scientific and engineering value.

The integration of molecular simulations and phase behavior experiments has emerged as the primary approach for investigating the properties of CO_2-philic surfactants. Sarbu et al. (2000) emphasized that high chain flexibility is a critical design criterion for CO_2-philic compounds, as it increases free volume and thereby enhances their CO_2 affinity. Acetylated isobutyl citrate (Zhang et al., 2024b), citrate A (Gong et al., 2025), and JU-series surfactants (Li et al., 2026) are all multi-ester-headgroup surfactants featuring flexible chain arrangements, and they exhibit favorable CO_2-philic properties. However, Potluri et al. (2003) and Ma et al. (2010) highlighted that spatial accessibility of ester groups to CO_2 constitutes a key metric for evaluating CO_2-philic performance. Cyclically arranged peracetylated monosaccharides and cyclodextrins demonstrate excellent CO_2 affinity owing to the outward-facing orientation of their ester groups, which facilitates contact with CO_2. Liao et al. (2020) and Ma et al., 2022a experimentally confirmed that cyclic arrangements of ester groups can likewise confer sufficient CO_2 affinity.

Although both linear (chain-like) and cyclic (ring-like) ester group arrangements have demonstrated CO_2-philic capability, a systematic comparison of their relative advantages and disadvantages in terms of CO_2-philic performance remains lacking. Therefore, in this work, multi-ester-headgroup surfactants featuring linear and cyclic ester arrangements were specifically designed to systematically investigate the dominant factors influencing CO_2 affinity in such compounds. In particular, the primary contributors to CO_2 affinity—such as the introduction of ester groups, their number, spatial arrangement, and related structural features—remain incompletely understood. In this study, a series of multi-ester headgroup surfactants (MEGs) were synthesized through acetylation and esterification, varying the number and arrangement of ester-containing side chains. Their chemical structures were characterized using Fourier transform infrared (FT-IR) and ^{1}H NMR spectroscopy. A laser-based apparatus was used to precisely measure the cloud point pressures of surfactants in CO_2. Molecular simulation techniques were applied to calculate solubility parameters and analyze the dominant intermolecular forces governing dissolution. The impact of spatial conformation was clarified through analysis of free volume and

chain segment dynamics. The key factors and mechanisms controlling the solubility of multi-ester headgroup surfactants in CO_2 were identified. This study expands the molecular library of hydrocarbon-based CO_2-philic surfactants, provides a theoretical basis for designing green, fluorine-free surfactants, and offers insights for reducing MMP and enhancing CO_2-EOR oil recovery.

2. Experimental methods

2.1. Materials

Carbon dioxide (CO_2, 99.99%) was purchased from Qingdao Xinkeyuan Gas Co., Ltd. Prior to use, CO_2 was purified by passage through a stainless-steel column (30 cm long, 1 cm in inner diameter) packed with activated 5 Å molecular sieves. Xylitol monolaurate (≥99.0%), sorbitol monolaurate (≥99.0%), lauryl glucoside (≥90%), sucrose dodecanoate (≥98%), octyl glucoside (≥90%), decyl glucoside (≥90%), and tetradecyl glucoside (≥90%) were purchased from Guangdong Yuanfeng Chemical Reagent Co., Ltd. Acetic anhydride (≥99.7%), perchloric acid (50%), triethylamine (≥99.7%), hydrochloric acid (32%), anhydrous sodium sulfate (≥99.7%), dodecanol (≥99.7%), chloroform (≥99.7%), and dichloromethane (≥99.7%) were purchased from Guoyao Chemical Reagent Co., Ltd. Sodium gluconate (≥99.7%) and sodium glucoheptonate (≥99.7%) were purchased from Shanghai McLean Biochemical Co., Ltd. *N*,*N*′-dicyclohexylcarbodiimide (DCC, ≥99%) and 4-dimethylaminopyridine (DMAP, ≥99%) were purchased from Shanghai Aladdin Biotechnology Co., Ltd. To eliminate the influence of moisture on the reactions, all reagents were dried prior to use. Specifically, reagents were stored over activated 5 Å molecular sieves for at least 10 h. The molecular sieves were activated by heating at 350 °C for 12 h.

2.2. Synthesis of multi-ester headgroup surfactants

Table 1 details the structures of multi-ester headgroup surfactants (MEG) designed in this study, comprising linear headgroup surfactants (MEG-L4, MEG-L5, MEG-L6) and cyclic headgroup surfactants (MEG-H3, MEG-H4, MEG-H7). Atom numbering in the structures follows the COMPASS III force field to differentiate atoms of the same type for pairwise interaction analysis.

2.2.1. Synthesis of MEG-L4, MEG-H3, MEG-H4, and MEG-H7

MEG-L4, MEG-H3, MEG-H4, and MEG-H7 were synthesized through complete acetylation of xylitol monolaurate, sorbitan monolaurate, lauryl glucoside, and sucrose laurate, respectively (Fan et al., 2005). Peracetylated octyl glucoside, decyl glucoside, and tetradecyl glucoside—featuring glucose units with fully acetylated hydroxyl groups and varying alkyl chain lengths (C_8, C_{10}, and C_{14})—were synthesized via complete acetylation of the corresponding alkyl glucosides. The acetylation procedure for polyhydroxy surfactants is exemplified using lauryl glucoside (Fig. 1).

In a three-neck round-bottom flask, acetic anhydride (50 mL) was cooled to 5 °C in an ice bath. To the cooled acetic anhydride, 50% perchloric acid (15 mmol, 3.01 g) and lauryl glucoside (30 mmol, 10.45 g) were added sequentially. The mixture was stirred under a nitrogen atmosphere at below 10 °C for 30 min. The reaction mixture was extracted twice with chloroform ($CHCl_3$, 0–2 °C), and the combined organic layers were washed with ice-cold water. After washing, water and triethylamine (3 mL) were added to the chloroform layer, followed by stirring for 12 h. The organic phase was separated, washed with dilute hydrochloric acid, and dried over anhydrous sodium sulfate (Na_2SO_4). Chloroform was removed under reduced pressure to yield the acetylated product, MEG-H4.

Table 1
The structural formula of multi-ester headgroup surfactants.

Name	Chemical structural formula
MEG-L4	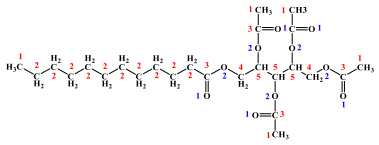
MEG-L5	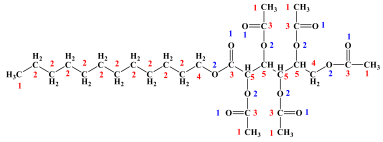
MEG-L6	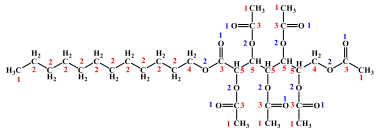
MEG-H3	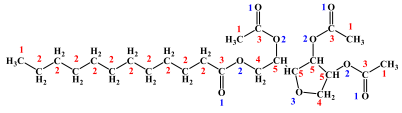
MEG-H4	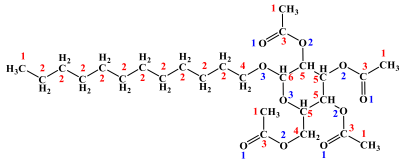
MEG-H7	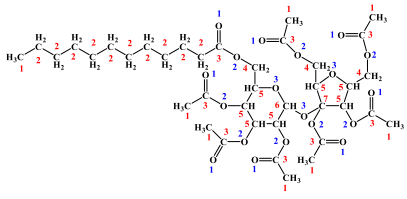

2.2.2. Synthesis of MEG-L5 and MEG-L6

MEG-L5 and MEG-L6 were synthesized through a two-step procedure. In the first step, hydroxyl groups of sodium gluconate or sodium glucoheptonate were completely acetylated as described in Section 2.2.1. In the second step, the acetylated acids were esterified with alcohols to yield multi-ester headgroup surfactants.

MEG-L5 was synthesized via Steglich esterification (Neises and Steglich, 1978). *N*,*N*′-dicyclohexylcarbodiimide (11 mmol, 2.27 g) and 4-(dimethylamino)pyridine (2 mmol, 0.25 g) were added to a three-neck round-bottom flask. Acetylated gluconic acid (10 mmol, 4.06 g) was dissolved in dichloromethane and introduced into the flask. The mixture was stirred at room temperature for 1 h to activate the acid. Dodecanol (10 mmol, 1.86 g), dissolved in dichloromethane, was added dropwise to the flask. After addition, the reaction mixture was stirred at room temperature for 18 h. The precipitated by-product dicyclohexylurea (DCU) was removed by filtration. The filtrate was washed with dilute hydrochloric acid until neutral pH, then dried over anhydrous sodium sulfate (Na_2SO_4) and filtered. The solvent was removed under reduced pressure to yield MEG-L5. The procedure for synthesizing MEG-L5 is illustrated in Fig. 2.

2.3. Characterization

The chemical composition and functional groups of multi-ester headgroup surfactants were analyzed using a Nicolet 6700 Fourier

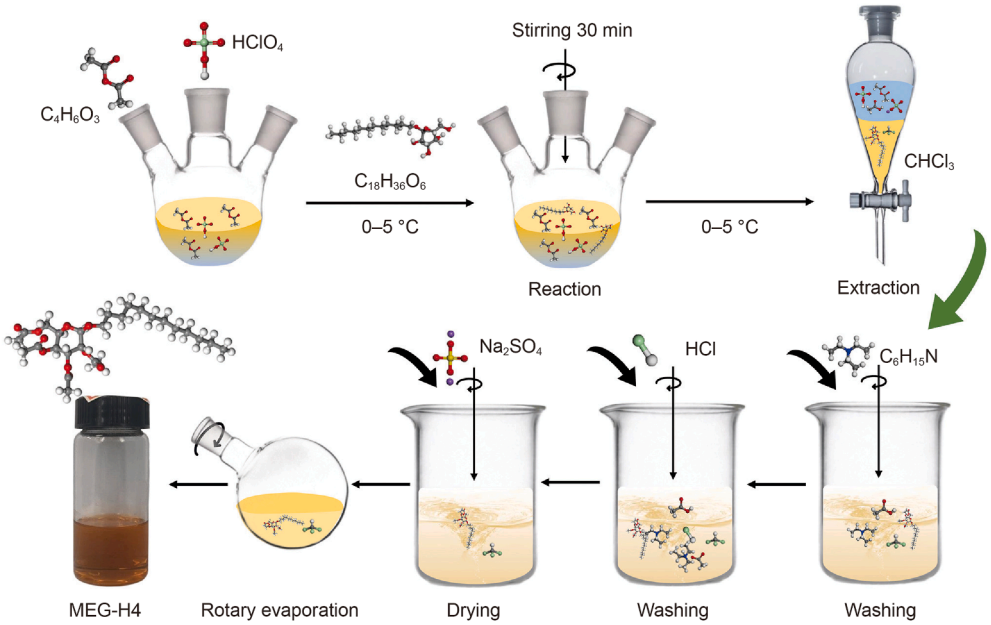

Fig. 1. The synthesis process of MEG-H4.

transform infrared spectrometer (Thermo Fisher Scientific, USA). Attenuated total reflectance (ATR) mode was used for all measurements. ^{1}H NMR spectra were recorded on an Agilent 400 MHz NMR spectrometer with deuterated chloroform ($CDCl_3$) as the solvent.

2.4. Solubility evaluation laser-light transmittance

To precisely measure surfactant solubility in CO_2, a custom semiconductor laser-based apparatus was designed and constructed to observe phase behavior (Fig. 3). Cloud point pressure of surfactants in supercritical CO_2 was measured by monitoring transmitted light power through a transparent visual reactor. A sharp change in transmitted light power signals the onset of surfactant separation from CO_2, defining the corresponding pressure as the cloud point pressure. All measurements were performed at 323.15 K with a surfactant concentration of 1 wt% relative to CO_2 mass. Using MEG-L5 as an example, the procedure is outlined as follows: (1) MEG-L5 was introduced into a sealed transparent reactor connected to the pipeline system. (2) A precisely measured amount of CO_2 was injected into an intermediate container, with its density and mass calculated from the temperature–pressure relationship (mass uncertainty: ±0.1 g). (3) CO_2 from the intermediate container was pumped into the visual reactor using an ISCO pump, and the pressure was increased until a transparent homogeneous phase was formed. (4) The semiconductor laser was activated, and transmitted light power through the reactor was monitored with a power meter. CO_2 was withdrawn from the intermediate container using the ISCO pump at a flow rate of 1 mL/min, gradually reducing system pressure until partial surfactant

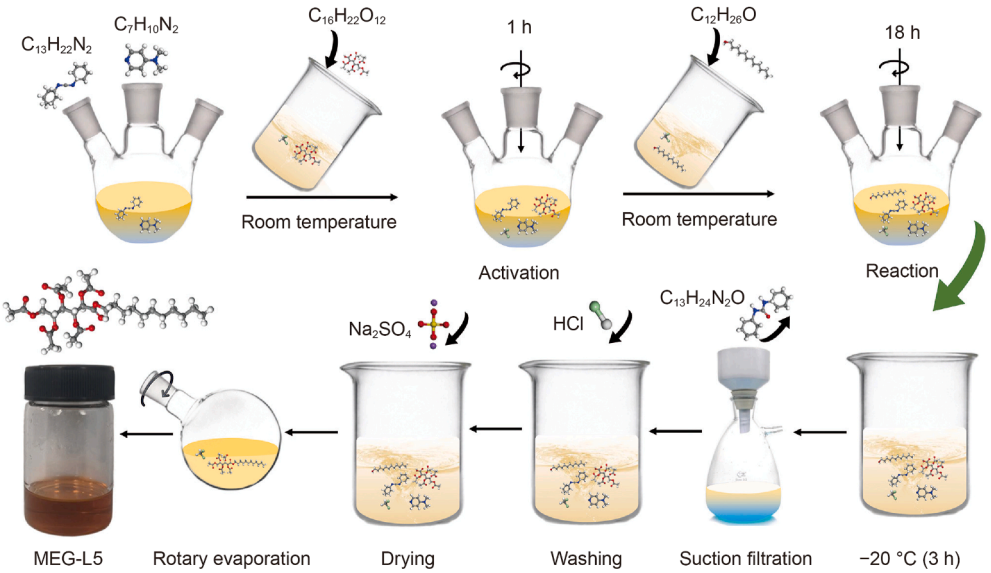

Fig. 2. The synthesis process of MEG-L5.

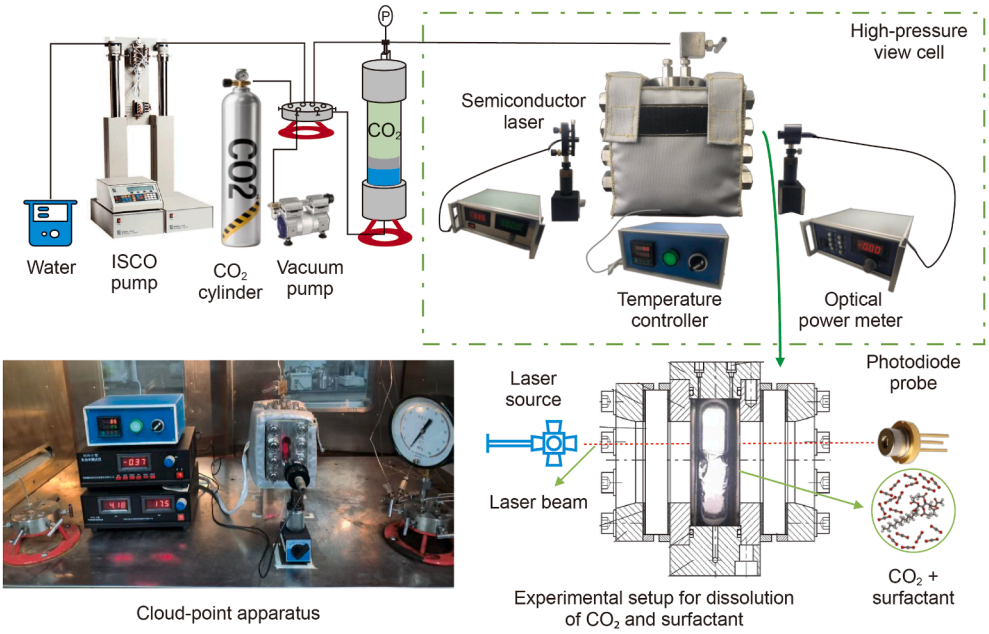

Fig. 3. Schematic diagram of the solubility evaluation apparatus.

separation occurred. Light power was recorded throughout the process. (5) A light power–pressure curve was generated, and its first derivative was calculated. The pressure at the maximum of the first derivative was designated as the cloud point pressure. Each system was measured in triplicate, and the average cloud point pressure was reported.

2.5. Details of molecular dynamics simulations

Molecular dynamics (MD) simulations were conducted using Materials Studio 2023 to elucidate the microscopic dissolution mechanisms of multi-ester headgroup surfactants in CO_2. The simulation procedure is outlined as follows: (1) Molecular modeling and force field assignment: Molecular structures were constructed, and force fields and charges were assigned using the Forcite module. The COMPASS III force field was applied to all systems, known for accurately predicting structural and thermodynamic properties of organic and inorganic compounds (Liu et al., 2015; Rigby et al., 1997; Yang et al., 2000). Charges were assigned using the default parameters of the COMPASS III force field. (2) Geometry optimization: Molecular structures were optimized to achieve stable conformations and energies. (3) Construction of simulation boxes: Simulation boxes, based on systems in Table 2, were built using the Amorphous Cell module. Each box had an initial density of 0.3 g/cm^3 and dimensions of 135 Å × 135 Å × 135 Å. Three-dimensional periodic boundary conditions were implemented. For each box, ten initial configurations were generated, with the lowest-energy configuration selected for further optimization. (4) The optimized configuration was annealed in five cycles from 298 to 498 K to eliminate local barriers. The temperature was increased and decreased five times during each cycle to minimize the global energy configuration. (5) MD simulation: Annealed models underwent MD simulation in two stages. First, a 10 ns equilibration phase was performed in the NVT ensemble with a 1.0 fs time step, using the Andersen thermostat for temperature control. Subsequently, a 2 ns production phase was conducted in the NPT ensemble at 323.15 K and 20 MPa with a 1.0 fs time step. Temperature and pressure were regulated using the Nosé thermostat and Berendsen barostat, respectively.

Table 2
Systems used in molecular simulations.

System	Composition	Number of surfactant molecules	Number of CO_2 molecules	$L_x \times L_y \times L_z$, Å
1	CO_2	0	10,000	135 × 135 × 135
2	MEG-L4	9	0	30 × 30 × 30
3	MEG-L5	8	0	30 × 30 × 30
4	MEG-L6	7	0	30 × 30 × 30
5	MEG-H3	10	0	30 × 30 × 30
6	MEG-H4	9	0	30 × 30 × 30
7	MEG-H7	6	0	30 × 30 × 30
8	CO_2 + MEG-L4	9	10,000	135 × 135 × 135
9	CO_2 + MEG-L5	8	10,000	135 × 135 × 135
10	CO_2 + MEG-L6	7	10,000	135 × 135 × 135
11	CO_2 + MEG-H3	10	10,000	135 × 135 × 135
12	CO_2 + MEG-H4	9	10,000	135 × 135 × 135
13	CO_2 + MEG-H7	6	10,000	135 × 135 × 135

Long-range electrostatic interactions were computed using the Ewald summation method, and van der Waals (vdW) interactions were calculated via atom-based summation with a 12.5 Å cutoff (medium). Snapshots of the six systems studied are presented in Fig. 4. The MD simulation results show good agreement with the experimental data (Tables S1 and S2 in Supporting Information), thereby validating the reliability of the MD model employed.

The surfactant concentration and experimental phase behavior concentration are both 1 wt%.

3. Results and discussion

3.1. Structural characterization of multi-ester headgroup surfactants

Multi-ester headgroup surfactants (MEG-L4, MEG-H3, MEG-H4, MEG-H7) were synthesized as shown in Fig. 1, while MEG-L5 and MEG-L6 were prepared as depicted in Fig. 2. Successful syntheses of all surfactants were confirmed using FT-IR and ^{1}H NMR spectroscopy.

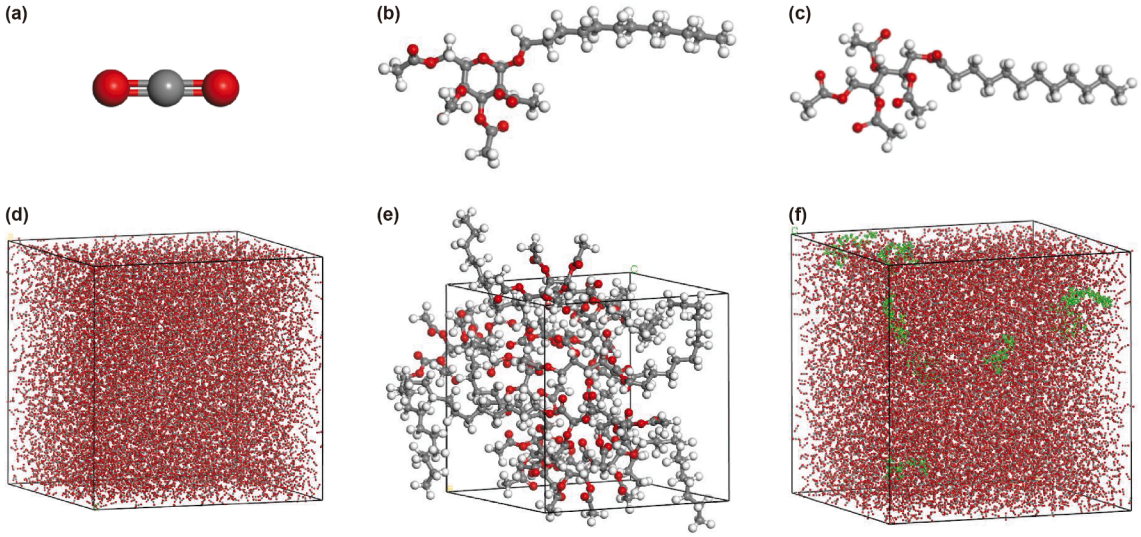

Fig. 4. Snapshots of the simulation boxes: (**a**) CO_2; (**b**) MEG-H4; (**c**) MEG-L4; (**d**) CO_2 system; (**e**) MEG-L4 system; (**f**) CO_2–MEG-L4 system.

Fig. 5(a) presents the FT-IR spectra of linear and cyclic multi-ester headgroup surfactants (MEG-L4, MEG-H3, MEG-H4, and MEG-H7). Sharp, intense peaks at 2923–2927 cm^{-1} were attributed to the asymmetric stretching vibration of $–CH_2–$ groups. Intense peaks at 1735–1745 cm^{-1} were assigned to the C=O stretching vibration of ester groups. Medium-intensity peaks at 1367–1371 cm^{-1} were attributed to the symmetric bending vibration of $–CH_3–$ groups. Intense peaks at 1213–1218 cm^{-1} were assigned to the C–O–C stretching vibration of esters, while medium-intensity peaks at 1034–1043 cm^{-1} corresponded to the symmetric C–O stretching vibration of ester groups. Fig. 5(b) shows the FT-IR spectra of MEG-L5 and MEG-L6. The acetylated gluconic acid precursor displayed a medium-intensity peak at 3216–3233 cm^{-1}, attributed to the –OH stretching vibration of carboxylic acids. After esterification, this peak vanished, and a peak at 2853 cm^{-1} emerged, assigned to the asymmetric stretching vibration of $–CH_2–$, confirming ester formation from carboxyl and hydroxyl groups. Sharp, intense peaks at 1741–1743 cm^{-1} and 1173–1184 cm^{-1} were assigned to the C=O and C–O–C stretching vibrations of ester groups, respectively. These FT-IR results confirm the successful synthesis of multi-ester headgroup surfactants. The FT-IR spectra of multi-ester-headgroup surfactants bearing alkyl chains of varying lengths are presented in Fig. S1 in Supporting Information.

Fig. 6 shows the ^1H NMR spectra of MEG series surfactants. Fig. 6(a) displays the ^1H NMR spectrum of acetylated gluconic acid. In the high-field region, a peak at 1.94 ppm was assigned to methyl group protons a, and two intense peaks at 1.97 ppm were attributed to methyl group protons b. These three methyl groups share the same chemical environment. A peak at 2.07 ppm, assigned to methyl group c, is slightly downfield due to deshielding by the adjacent carboxylic acid. A multiplet at 4.11 ppm (integral = 2) was assigned to methylene protons d. Peaks at 4.96 and 5.19 ppm were assigned to tertiary protons e and f, while multiplets at 5.39 and 5.52 ppm were attributed to tertiary protons g and h. Proton g, deshielded by an adjacent oxygen atom, exhibits a downfield shift.

Fig. 6(b) displays the ^1H NMR spectrum of MEG-L5. In the high-field region, a multiplet at 0.87 ppm was assigned to terminal methyl protons a. A peak at 1.25 ppm was assigned to methylene protons b, and peaks at 1.47 and 1.61 ppm were attributed to methylene protons c and d. Multiplets from 2.12 to 1.90 ppm

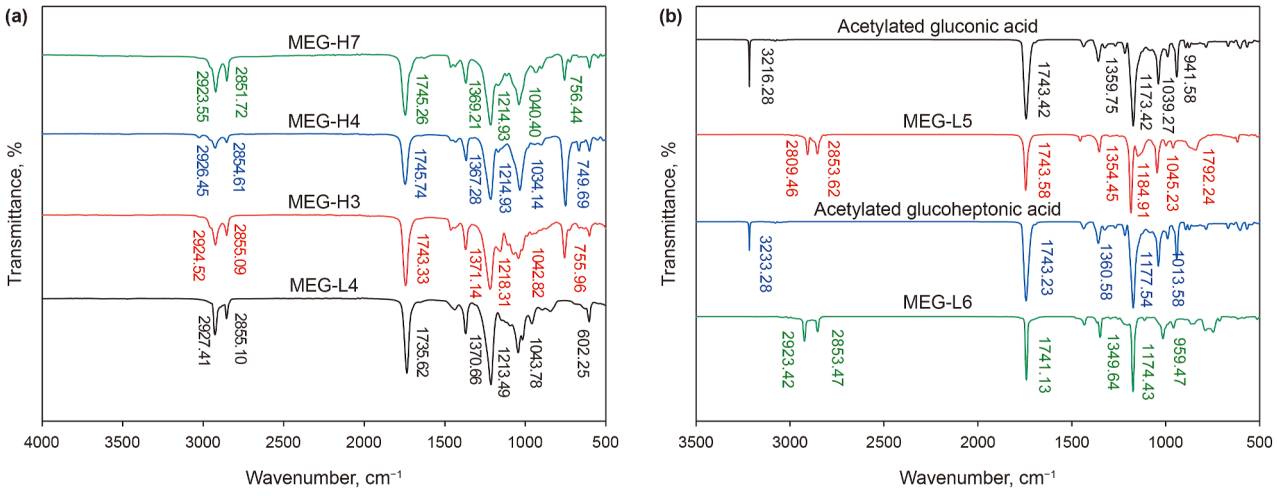

Fig. 5. FT-IR spectra of MEG surfactants.

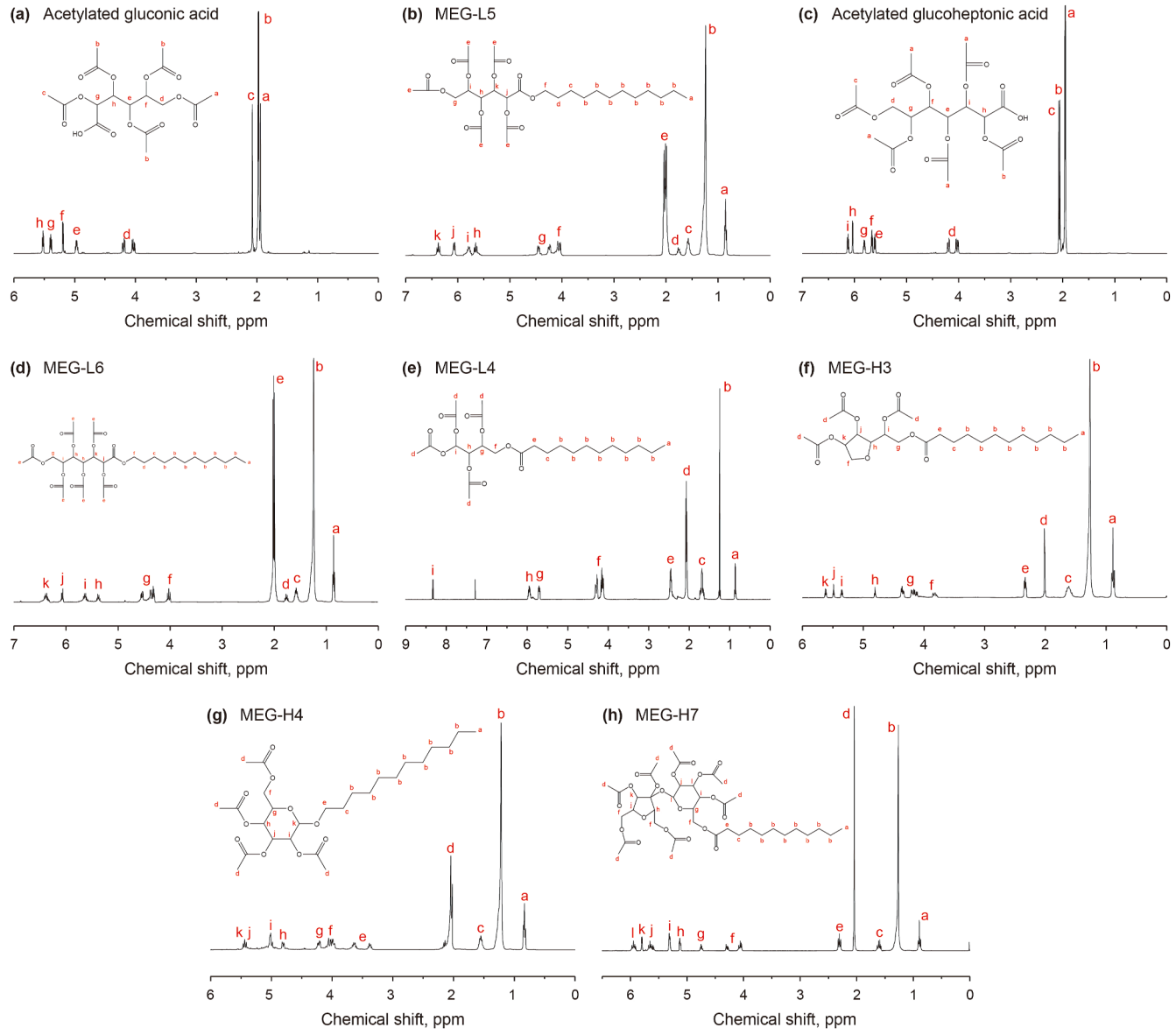

Fig. 6. ^{1}H NMR spectra of MEG surfactants.

(integral = 15) were assigned to five equivalent methyl group sets. Signals at 4.07 and 4.51–4.20 ppm were assigned to methylene protons f and g, deshielded by adjacent oxygen atoms. A peak at 5.66 ppm (integral = 1) was assigned to proton h, with peaks at 5.57, 6.05, and 6.39 ppm attributed to protons i, j, and k, respectively, all shifted downfield due to oxygen deshielding.

Combined FT-IR and ^{1}H NMR analyses confirmed the successful synthesis of MEG-L5. The ^{1}H NMR spectra of MEG-L4, MEG-L6, MEG-H3, MEG-H4, MEG-H7, and other multi-ester-headgroup surfactants bearing alkyl chains of varying lengths are presented in Fig. S2 in Supporting Information.

3.2. Dissolution behavior of multi-ester headgroup surfactants in CO_2

To evaluate the solubility of multi-ester headgroup surfactants in CO_2, the phase behavior of surfactant–CO_2 binary systems was studied using a high-pressure, high-temperature visual reactor (Fig. 2).

3.2.1. Phase behavior of surfactant–CO_2 binary systems

Fig. 7 depicts the phase behavior of the MEG-L5–CO_2 system at 323.15 K. With increasing pressure, gaseous CO_2 occupied the upper reactor, while CO_2 at the bottom liquefied, forming a clear gas–liquid interface (Fig. 7(a)). At 9 MPa, CO_2 in the reactor reached a supercritical state, appearing viscous at the bottom (Fig. 7(b)). At this stage, MEG-L5 began dissolving in supercritical CO_2 ($scCO_2$), reflecting enhanced CO_2 solvation capacity with increasing pressure (Lemaire et al., 2022). At 16 MPa, MEG-L5 fully dissolved in CO_2, rendering the reactor clear and transparent (Fig. 7(c)). During depressurization, turbidity emerged at 9.5 MPa (Fig. 7(d)), signaling the onset of MEG-L5 phase separation from the homogeneous system. At 4 MPa, most MEG-L5 had separated from CO_2, with liquid CO_2 accumulating at the reactor bottom (Fig. 7(e)). At 1 MPa, bubble formation, resembling boiling water, was observed in the reactor groove (Fig. 7(g)), due to CO_2 escaping from MEG-L5. Upon further depressurization to 0 MPa, precipitated MEG-L5 was evident in the reactor groove (Fig. 7(h)), confirming its high CO_2 solubility.

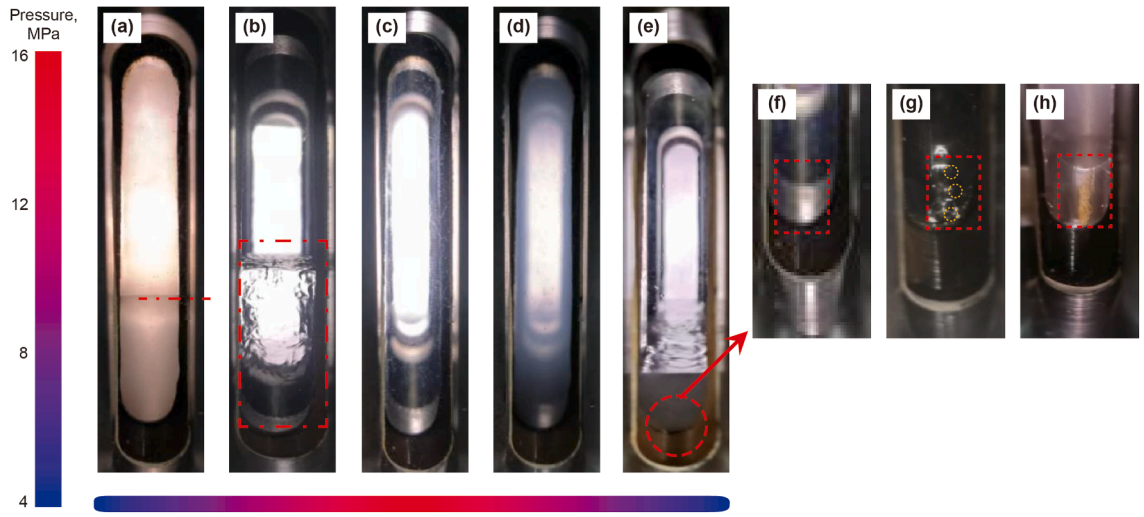

Fig. 7. Phase behavior of MEG-L5 + CO_2 system (323.15 K).

3.2.2. Effect of ester group number and arrangement on the solubility of multi-ester headgroup surfactants in CO_2

Ester groups are known to exhibit high CO_2-philicity (Liao et al., 2020; Zhang et al., 2024b; Ma et al., 2022a). The number and spatial arrangement of CO_2-philic ester groups significantly influence the solubility of multi-ester headgroup surfactants in CO_2. Fig. 8(a) depicts the variation in transmitted light power with pressure for surfactant–CO_2 systems at 1 wt% concentration. Above 14 MPa, the transmitted light power stabilized, indicating a homogeneous, transparent binary system. As the pressure approached the phase transition point, the transmitted light power decreased sharply, indicating partial surfactant precipitation and the formation of a two-phase system.

Fig. 8(b) shows the first derivative of transmitted light power with respect to pressure, where the extrema correspond to the cloud point pressure of each surfactant. The cloud point pressure increases in the following order: MEG-L5 < MEG-L4 < MEG-L6 < MEG-H4 < MEG-H3 < MEG-H7. These results yield two conclusions: (1) The arrangement of CO_2-philic ester groups strongly influences CO_2 solubility, with linear arrangements outperforming cyclic ones. (2) For a given arrangement, the cloud point pressure initially decreases and then increases with the number of ester groups, suggesting an optimal ester density for maximizing CO_2 solubility. This trend is consistent with the findings of Potluri et al. (2002). Therefore, rational selection of both the number and the spatial arrangement of ester groups in the CO_2-philic headgroup is crucial for the design and optimization of hydrocarbon-based CO_2-philic surfactants.

Table 3 summarizes the cloud point pressures of representative hydrocarbon-based CO_2-philic surfactants at specified temperatures and concentrations. Among the surfactants compared, the multi-ester headgroup surfactants exhibit the lowest cloud point pressures under identical temperature and concentration conditions, indicating superior CO_2 solubility. These multi-ester headgroup surfactants dissolve completely in CO_2 at pressures below 12 MPa, a value substantially lower than the typical MMP required for CO_2 miscible flooding in most Chinese reservoirs (20–30 MPa (Lv et al., 2022)). Consequently, multi-ester headgroup surfactants show promising potential for application in CO_2-enhanced oil recovery processes.

3.2.3. Effect of temperature on the solubility of multi-ester-headgroup surfactants in CO_2

Using MEG-L5 as a representative example, the temperature dependence of solubility for multi-ester headgroup surfactants in CO_2 was evaluated via cloud point pressure measurements. As

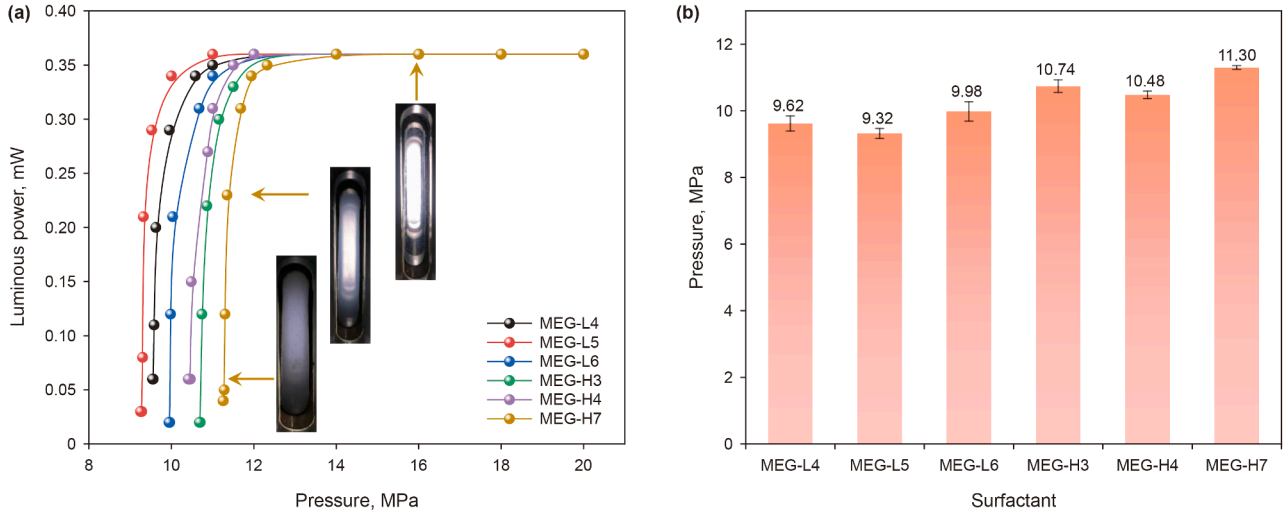

Fig. 8. Dissolution performance of MEG surfactant–CO_2 systems. (**a**) Variation in transmitted light power with pressure. (**b**) Cloud point pressures of MEG surfactant–CO_2 systems.

Table 3
Cloud point pressures of surfactants in relevant literature.

Surfactant	Concentration, wt%	Temperature, K	Cloud pressure, MPa
Polyether (AEO_3) (Xu et al., 2025)	1	308.15	13.50
Alkyl block polyether (C_4PO_3) (Lv et al., 2020)	0.4	323.15	10.12
Multiester (6JU12) (Li et al., 2026)	0.25	333	10.80
Polyoxyethylene polyoxypropylene ether ($C_4EO_3PO_3$) (Zhang et al., 2024a)	1	323	14.00
MEG-L5	1	323.15	9.32

illustrated in Fig. 9, the cloud point pressure rises with increasing temperature, indicating that higher temperatures reduce surfactant solubility in CO_2. This trend stems mainly from the fact that increasing temperature substantially decreases the density of supercritical CO_2, on which its solvation power strongly depends. Higher CO_2 density strengthens dispersion forces and specific solute–solvent interactions (e.g., LA–LB interactions) between CO_2 and the surfactant. Consequently, within a fixed pressure range, the temperature-driven density reduction markedly diminishes the solvation capability of CO_2. Detailed examination indicates that the cloud point pressure increases relatively slowly with temperature in the range of 308.15–323.15 K (9.02–9.32 MPa), whereas the rate becomes markedly steeper above 323.15 K (323.15–333.15 K). This change in slope arises from the competing effects of temperature: a reduction in CO_2 density (detrimental to solubility) versus an increase in surfactant molecular thermal motion/kinetic energy (favorable to solubility). Enhanced thermal motion enables surfactant molecules to overcome intermolecular cohesive forces and facilitates greater dispersion, thereby positively contributing to solubility. In the lower temperature range (308.15–323.15 K), the favorable effect of increased surfactant thermal motion largely offsets the adverse impact of decreasing CO_2 density, resulting in a relatively gradual increase in cloud point pressure. At higher temperatures (>323.15 K), however, the detrimental effect of CO_2 density reduction dominates, outweighing the benefit of enhanced thermal motion and producing a much steeper rise in cloud point pressure.

3.2.4. Effect of alkyl chain length on the solubility of multi-ester headgroup surfactants in CO_2

The CO_2-philic headgroup of multi-ester headgroup surfactants consists primarily of ester groups, whereas the lipophilic tail comprises linear alkyl chains of varying lengths. As CO_2-phobic moieties, these alkyl chains inevitably influence the overall CO_2 solubility of these surfactants. Therefore, the impact of alkyl chain lengths (C_8, C_{10}, C_{12}, and C_{14}) on the CO_2 solubility of the cyclic multi-ester headgroup surfactant MEG-H4 was systematically investigated, as shown in Fig. 10.

Under identical experimental conditions, the cloud point pressure of the MEG-H4–CO_2 binary system increases with increasing alkyl chain length. When the alkyl chain reaches C_{14}, the cloud point pressure reaches 10.72 MPa, demonstrating that longer alkyl chains exert a negative effect on surfactant solubility in CO_2. In the C_8–C_{12} range, the cloud point pressure increases gradually, suggesting that the strong CO_2 affinity of the multi-ester headgroup largely compensates for the detrimental influence of increasing chain length. However, extending the chain to C_{14} raises the cloud point pressure sharply to 11.34 MPa, revealing that the adverse effect of the alkyl tail becomes dominant and causes a pronounced discontinuity in the trend. This suggests the existence of an optimal alkyl chain length range for a given CO_2-philic headgroup structure. For multi-ester headgroup surfactants, alkyl chain lengths exceeding C_{12} appear to compromise the balance between CO_2 solubility and molecular amphiphilicity. Thus, an appropriate alkyl chain length must provide sufficient lipophilicity while maintaining relatively low cloud point pressures in CO_2. Accordingly, judicious selection of alkyl chain length is critical for the design and optimization of hydrocarbon-based CO_2-philic surfactants.

3.3. Effect of interaction energy on the solubility of multi-ester headgroup surfactants

The dissolution of surfactants in CO_2 is a thermodynamic equilibrium process governed by enthalpy and entropy. From an enthalpic perspective, enthalpy change drives dissolution, reflecting net changes in intermolecular interaction energy.

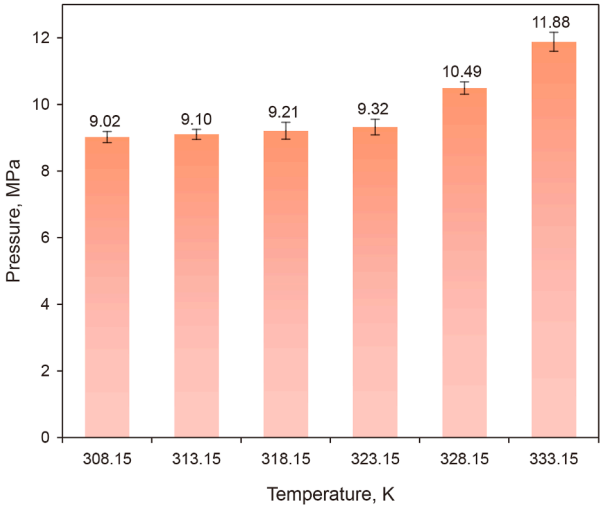

Fig. 9. Effect of temperature on cloud point pressure.

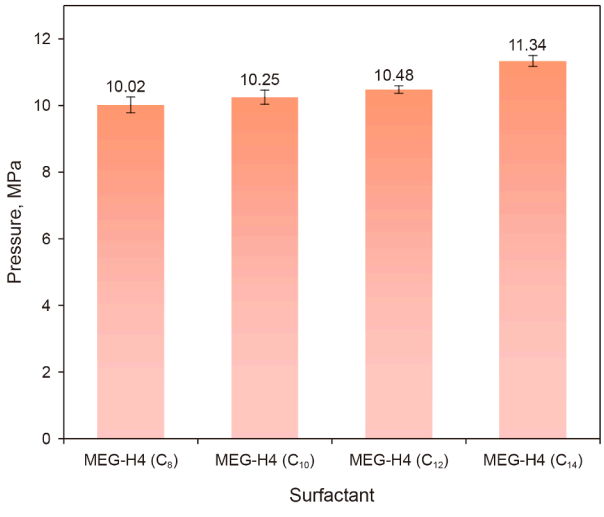

Fig. 10. Effect of alkyl chain length on cloud point pressure.

Parameters including solubility parameters, interaction energies, and intermolecular forces offer insights into the enthalpic contribution.

3.3.1. Solubility parameter

The solubility parameter is a critical metric for predicting solute solubility in a solvent, as proposed by Hildebrand and Scott (1950). The solubility parameter, defined as the square root of the cohesive energy density (Hansen, 1969), is calculated as follows:

$$\delta = \sqrt{e_{coh}} = \sqrt{\frac{E_{coh}}{V}} \tag{1}$$

where δ is the solubility parameter; e_{coh} is the cohesive energy density; E_{coh} is the cohesive energy; and V is the volume of the simulation box.

Thermodynamic studies show that spontaneous surfactant dissolution in CO_2 requires a negative Gibbs free energy change.

$$\Delta G_{mix} = \Delta H_{mix} - T\Delta S_{mix} < 0 \tag{2}$$

where ΔH_{mix} represents the enthalpy change of mixing; ΔS_{mix} represents the entropy change of mixing; and T is the absolute temperature. During dissolution, molecular arrangements tend toward disorder, resulting in $\Delta S_{mix} > 0$. Consequently, spontaneous surfactant dissolution in CO_2 is primarily driven by ΔH_{mix}. The relationship between mixing enthalpy and solubility parameters is expressed in Eq. (3):

$$\Delta H_{mix} = V_m \phi_a \phi_b \left(\sqrt{e_{coh1}} - \sqrt{e_{coh2}}\right)^2 = V_{mix} \phi_a \phi_b (\delta_a - \delta_b)^2 \tag{3}$$

where V_m is the molar mixing volume; subscripts "a" and "b" represent the solvent and solute, respectively; ϕ is the volume fraction of each component. Eq. (3) indicates that the closer the solubility parameters between solvent and solute, the lower the mixing enthalpy, facilitating dissolution.

Solubility parameter differences ($\Delta\delta$) are presented in Table 4. The $\Delta\delta$ values between CO_2 and multi-ester headgroup surfactants follow the order: MEG-L5 < MEG-L4 < MEG-L6 < MEG-H4 < MEG-H3 < MEG-H7, indicating that MEG-L5, with five linearly arranged ester groups, exhibits the highest CO_2 compatibility. Under fixed ester group arrangement, increasing the number of ester groups initially reduces the difference in solubility parameters (δ) between the surfactant and CO_2, followed by an increase. This corresponds to an initial enhancement followed by a decline in CO_2 affinity, in agreement with Potluri's observation (Potluri et al., 2002) that CO_2 affinity is maximized at an optimal ester group density in the molecule. Both MEG-L4 and MEG-H4 contain four ester groups, with linear arrangement in MEG-L4 and cyclic in MEG-H4. The $\Delta\delta$ values show that linear ester arrangements exhibit greater CO_2-philicity than cyclic ones, highlighting spatial arrangement of CO_2-philic ester groups as a key factor in CO_2 affinity. Greenhalgh et al. (1999) states that substances with $\Delta\delta < 7.0$ $(J/cm^3)^{-0.5}$ are highly miscible, while $\Delta\delta > 10$ $(J/cm^3)^{-0.5}$ indicates poor miscibility. The results demonstrate that multi-ester headgroup surfactants exhibit excellent solubility in CO_2. Phase behavior experiments reveal that these surfactants dissolve completely in CO_2 at pressures below 12 MPa and a concentration of 1 wt%. This value is substantially lower than the typical MMP in Chinese reservoirs, which generally exceeds 20 MPa. These findings indicate that multi-ester headgroup surfactants possess promising potential for application in CO_2-enhanced oil recovery. Concurrently, the good agreement between simulation and experimental results confirms the capability of MD simulations to accurately describe and predict the miscibility of these surfactants with CO_2.

Table 4
Cohesive energy density and solubility parameters of different systems (323.15 K, 20 MPa).

No.	System	e_{coh}, J/m^3	δ, $(J/cm^3)^{-0.5}$	$\Delta\delta$, $(J/cm^3)^{-0.5}$
1	CO_2	1.595×10^8	12.629	0
2	MEG-L4	3.390×10^8	18.411	5.782
3	MEG-L5	3.347×10^8	18.293	5.664
4	MEG-L6	3.406×10^8	18.455	5.826
5	MEG-H3	3.478×10^8	18.650	6.021
6	MEG-H4	3.444×10^8	18.558	5.929
7	MEG-H7	3.513×10^8	18.741	6.112

3.3.2. Interaction energy of MEG–CO_2 systems

Interaction energy directly indicates the affinity of surfactants for CO_2 (Lv et al., 2023; Zhang et al., 2024a). Fig. 11(a) and (b) show intermolecular interaction energies in multi-ester headgroup surfactant–CO_2 binary systems. The surfactant–surfactant interaction energies range from −82.56 to −162.39 kcal/mol, which are significantly less negative than the surfactant–CO_2 interaction energies (from −435.15 to −387.25 kcal/mol). This suggests that multi-ester headgroup surfactants exhibit weak self-interactions, aligning with Sarbu's design principle (Sarbu et al., 2000) that excessive solute–solute interaction energies impair solubility. In Fig. 11(a), the surfactant–surfactant interaction energy becomes progressively more negative (stronger attraction) with increasing ester group number from MEG-L4 to MEG-L6, reaching a maximum magnitude of −435.15 kcal/mol for MEG-L6. This trend appears inconsistent with the experimental cloud point pressure behavior of the linear multi-ester headgroup surfactants, which first decreases and then increases, with MEG-L5 exhibiting the lowest value (9.32 MPa) compared to MEG-L6 (9.98 MPa). In contrast, for the cyclic multi-ester headgroup surfactants (MEG-H3 to MEG-H7), the surfactant–surfactant interaction energy first becomes more negative and then less negative with increasing ester group number (Fig. 11(b)), peaking at −410.25 kcal/mol for MEG-H4. This non-monotonic trend aligns well with the solubility behavior as characterized by cloud point pressures.

To compare molecular interaction strengths within the same system, an energy increment ratio was defined. The energy increment ratio is calculated for a reference system as follows:

$$X = \frac{E_n - E}{E} \times 100\% \tag{4}$$

where X is the energy increment ratio, %; E_n is the interaction energy of the comparison system, kcal/mol; and E is the interaction energy of the reference system, kcal/mol. For linear multi-ester headgroup surfactants, MEG-L4 was the reference, while for cyclic multi-ester headgroup surfactants, MEG-H3 was used.

In linear ester headgroup surfactant–CO_2 binary systems (Fig. 11(a)), increasing ester group number reduces CO_2–CO_2 interaction energy by < 2% and increases surfactant–CO_2 interaction energy by < 3%. In contrast, surfactant–surfactant interaction energy increases by up to 80%. This suggests that increasing ester group number slightly disrupts CO_2 aggregation, but surfactant aggregation persists, competing with surfactant–CO_2 interactions and reducing CO_2 solubility. These results suggest that simply increasing the number of CO_2-philic groups (ester moieties) does not necessarily enhance overall CO_2 solubility, analogous to the behavior reported for amino-group-containing compounds (Zhang et al., 2021). This explains why MEG-L6 shows stronger

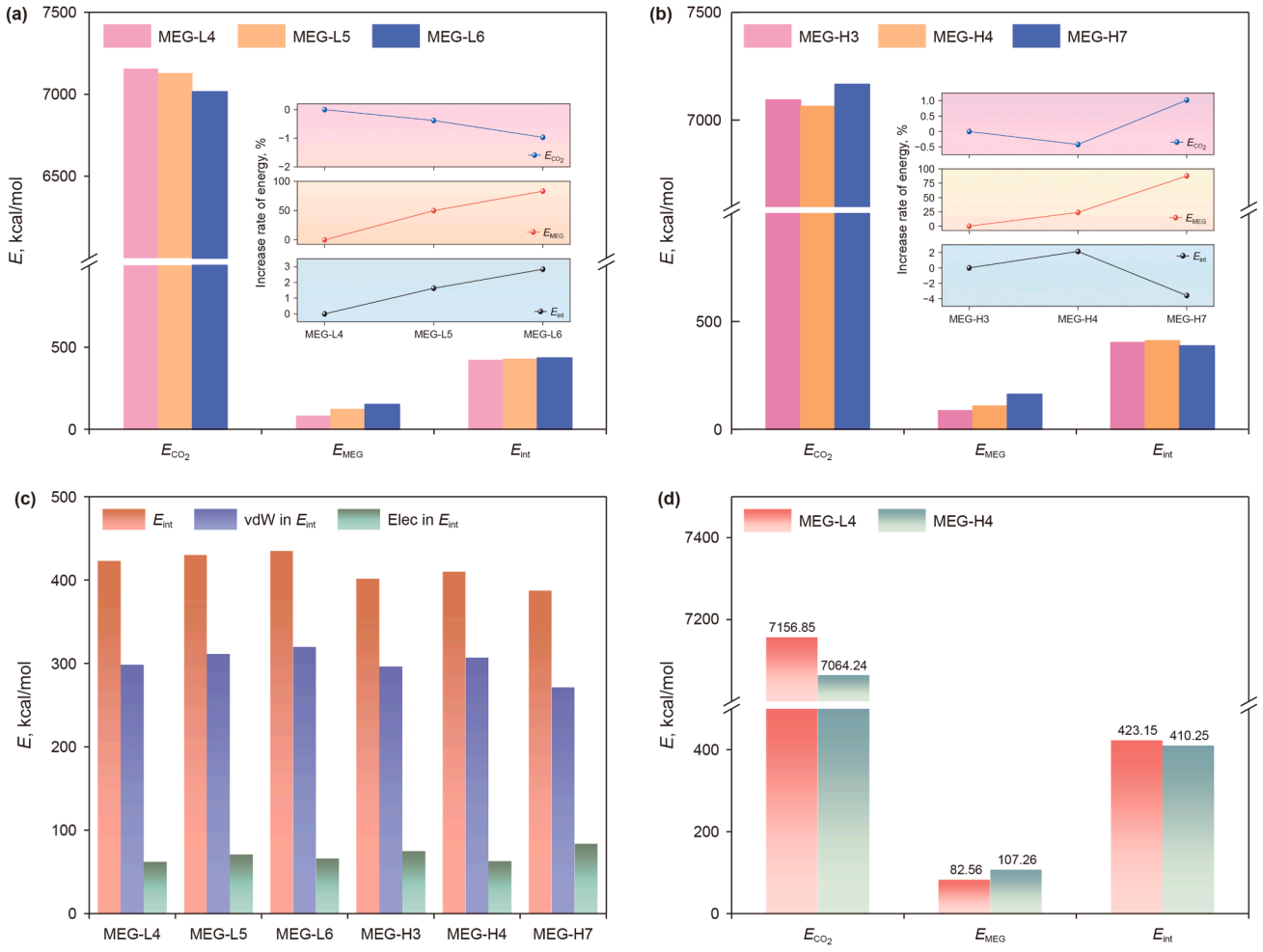

Fig. 11. Interaction energies in binary systems. (**a**) Interaction energies of linear ester headgroup surfactant–CO_2 systems. (**b**) Interaction energies of cyclic ester headgroup surfactant–CO_2 systems. (**c**) Components of interaction energies in binary systems. (**d**) Comparison of interaction energies between linear and cyclic ester headgroup surfactants. E_{CO_2} represents the interaction energy between CO_2 molecules; E_{MEG} represents the interaction energy between MEG molecules; E_{int} represents the interaction energy between CO_2 and MEG molecules.

surfactant–CO_2 interactions than MEG-L5, yet exhibits a higher cloud point pressure. The additional ester group leads to a greater increase in the magnitude of surfactant–surfactant interaction energy compared to the increase in surfactant–CO_2 interaction energy. In the cyclic surfactant–CO_2 binary system (Fig. 11(b)), the CO_2–CO_2 intermolecular interaction energy first becomes less negative and then more negative (variation within 2%), whereas the surfactant–CO_2 interaction energy first becomes more negative and then less negative (variation of 3.59%). Meanwhile, the surfactant–surfactant interaction energy becomes dramatically more negative, increasing in magnitude by 87.68% at MEG-H7. This suggests that the cyclic arrangement of ester groups promotes surfactant self-aggregation, especially at higher ester group numbers (MEG-H7), thereby significantly impairing CO_2 solubility. Fig. 11(c) indicates that interaction energy between multi-ester headgroup surfactants and CO_2 primarily comprises van der Waals (vdW) and electrostatic forces, with vdW contributions exceeding 70%, underscoring their dominant role in CO_2 affinity. Fig. 9(d) compares linear and cyclic ester arrangements with the same ester group number, revealing stronger interaction energies for linear arrangements (|–423.15| kcal/mol > | –410.25| kcal/mol). These findings support the following conclusions: Linear CO_2-philic ester group arrangements yield stronger surfactant–CO_2 interaction energies. An optimal ester group number maximizes surfactant–CO_2 interactions, while excessive ester groups enhance surfactant–surfactant interactions, competing with surfactant–CO_2 interactions. Interaction energy between multi-ester headgroup surfactants and CO_2 is primarily driven by vdW and electrostatic forces, with vdW forces dominating.

3.3.3. *RDFs of multi-ester headgroup surfactants–CO_2*

To clarify the role of specific atoms in multi-ester headgroup surfactants' CO_2 affinity, RDFs of atom pairs were analyzed (Lv et al., 2023; Thompson et al., 2022). RDFs reveal molecular aggregation and interaction patterns within the system, offering insights into microscopic structure. Atom numbering for C, O, and H in surfactants is presented in Table 1.

RDF results (Fig. 12(a)) indicate that CO_2 carbon atoms primarily aggregate around surfactant carbon atoms at 4.29–5.16 Å, which is consistent with van der Waals interaction ranges (Small, 1953). Among these, C_1 (methyl carbon) shows the shortest distance (4.29 Å) to CO_2 carbon with the highest RDF peak, suggesting preferential accumulation around the terminal methyl group. Fig. 12(b) presents RDFs of surfactant carbon atoms with CO_2 oxygen atoms, with peaks at 3.93–4.95 Å. Shorter interaction distances indicate stronger C–O interactions than C–C interactions, as CO_2 oxygen acts as a Lewis base (LB) donating lone pair electrons, while surfactant carbon atoms serve as Lewis acids (LA), forming

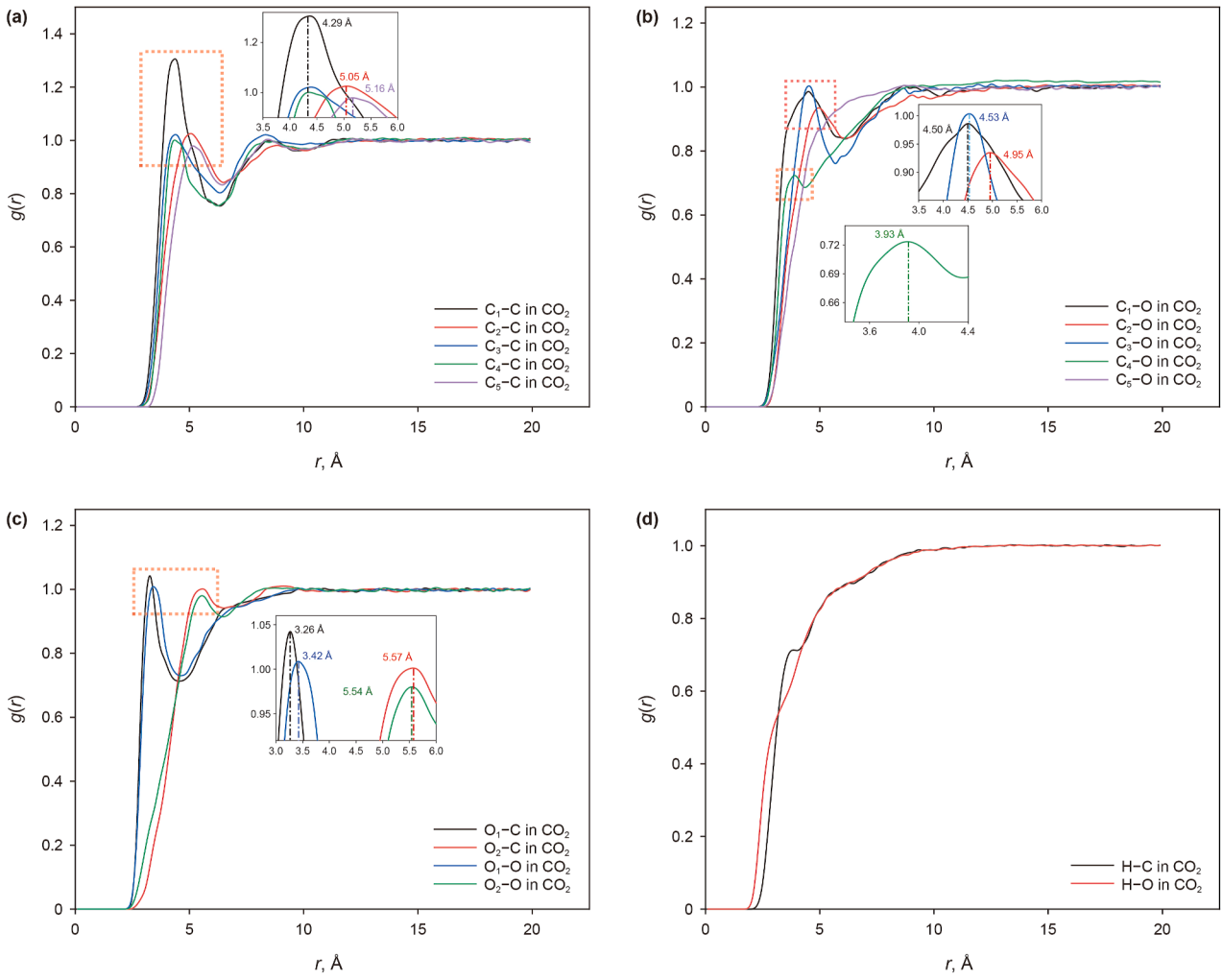

Fig. 12. RDFs between atoms in MEG-L5 and atoms in CO_2. (**a**) C in MEG-L5–C in CO_2; (**b**) C in MEG-L5–O in CO_2; (**c**) O in MEG-L5–CO_2; (**d**) H in MEG-L5–CO_2.

LA–LB interactions. The C_4 atom, bonded to the ester group, carries a partial positive charge due to the carbonyl oxygen's electron-withdrawing effect, leading to stronger C_4–O interactions (3.93 Å). However, steric hindrance reduces contact frequency, resulting in a lower RDF peak. Fig. 12(c) shows RDFs of surfactant oxygen atoms with CO_2 carbon and oxygen atoms. The carbonyl oxygen O_1 shows RDF peaks at 3.26 Å (with CO_2 carbon) and 3.42 Å (with CO_2 oxygen). In O_1–C pairs, O_1 acts as a LB donating lone pair electrons, while CO_2 carbon acts as a LA with an empty orbital, forming LA–LB interactions; O_1–O pairs are governed by dispersion forces. The carbonyl's electron-withdrawing effect weakens the ester C–O bond compared to ethers, leading to weaker O_2 (ester ether oxygen)–CO_2 C/O interactions, with RDF peaks at 5.54 and 5.57 Å. Fig. 12(d) indicates that surfactant hydrogen atoms lack significant RDF peaks with CO_2, suggesting no specific interactions.

These findings support the following conclusions: (1) LA–LB interactions and dispersion forces primarily drive surfactant–CO_2 interactions, with LA–LB interactions being stronger. (2) Terminal methyl carbons engage in strong dispersion and LA–LB interactions with CO_2, explaining enhanced CO_2 solubility with chain-end methylation (Mohamed et al., 2015). (3) O_1 (carbonyl oxygen in ester groups) interacts with CO_2 carbon and oxygen via LA–LB and dispersion forces, enhancing CO_2 affinity, while O_2 (ester ether oxygen) interacts weakly but stabilizes CO_2 binding to the ester group (Hu et al., 2015). (4) Ester and terminal methyl groups are effective CO_2 binding sites.

3.3.4. *Effect of ester group number/configuration on interactions*

Fig. 13 compares the aggregation behavior of specific atoms in different surfactants with CO_2. CO_2 primarily aggregates around the C_1 atom at 4.29 Å through dispersion forces. With increasing ester group number, C_1–C dispersion interactions initially increase, then decrease. Cyclic surfactants show a similar trend (Fig. 13(a)), with MEG-L5 exhibiting the highest RDF peak. C_2 and C_3 exhibit the same trend. For C_4, the trend is consistent, but peak positions vary as follows: MEG-L4 > MEG-L5 > MEG-L6, MEG-H3 = MEG-H4 > MEG-H7. This suggests that surfactants with fewer ester groups exhibit stronger interactions. C_4, bonded to the ester's ether oxygen, faces increased steric hindrance with more CO_2-philic ester groups, reducing CO_2 contact and interaction strength. Only in linear ester surfactants does the C_5 atom show a detectable peak with CO_2 carbon atoms; no C_5–C peaks are observed in cyclic surfactants. Analysis of C_5 positions in cyclic surfactants reveals its location on the rigid ring backbone, limiting CO_2 contact and contributing minimally to CO_2 affinity. Similarly, MEG-H4 and MEG-H7 possess a C_6 atom absent in other surfactants. Statistical analysis reveals no C_6–CO_2 carbon RDF peak, due to its embedding in the rigid backbone. These findings support the following

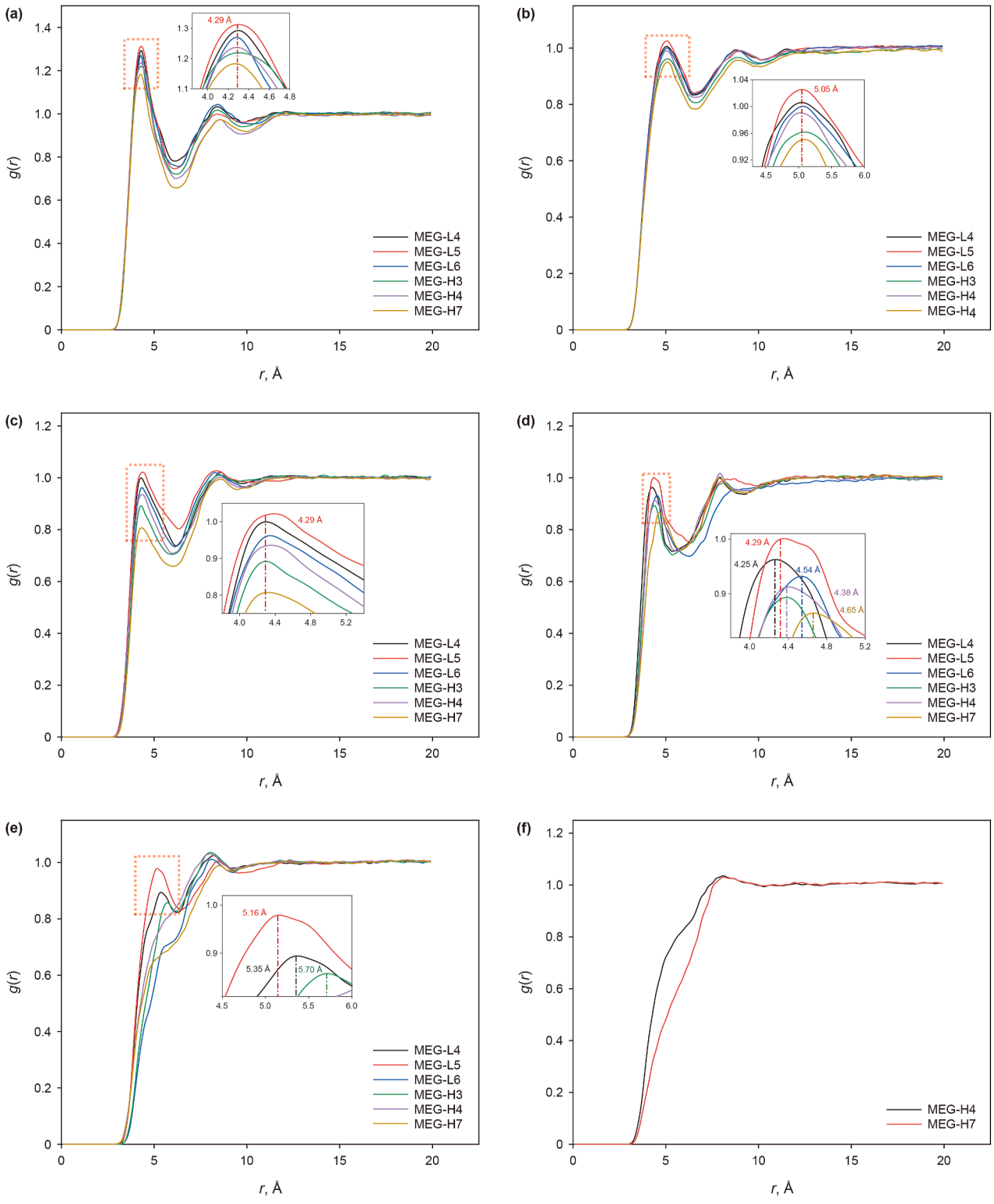

Fig. 13. RDFs between C atoms in MEG surfactants and C atoms in CO_2. (**a**) C_1–C in CO_2; (**b**) C_2–C in CO_2; (**c**) C_3–C in CO_2; (**d**) C_4–C in CO_2; (**e**) C_5–C in CO_2; (**f**) C_6–C in CO_2.

conclusions: (1) An optimal ester group number maximizes dispersion interactions between surfactant carbon and CO_2 carbon atoms. (2) Cyclic multi-ester headgroup surfactants are less effective at promoting C–CO_2 dispersion interactions than linear arrangements. (3) Steric hindrance significantly limits dispersion interactions between surfactant carbon atoms and CO_2.

Fig. 14 presents interactions between carbon atoms in multi-ester headgroup surfactants and CO_2 oxygen atoms. For C_1–C_4, the trend is as follows: MEG-L5 > MEG-L4 > MEG-L6 > MEG-H4 > MEG-H3 > MEG-H7, showing that LA–LB interactions between surfactant C_1–C_4 and CO_2 oxygen atoms initially increase, then decrease with increasing ester group number. Linear ester

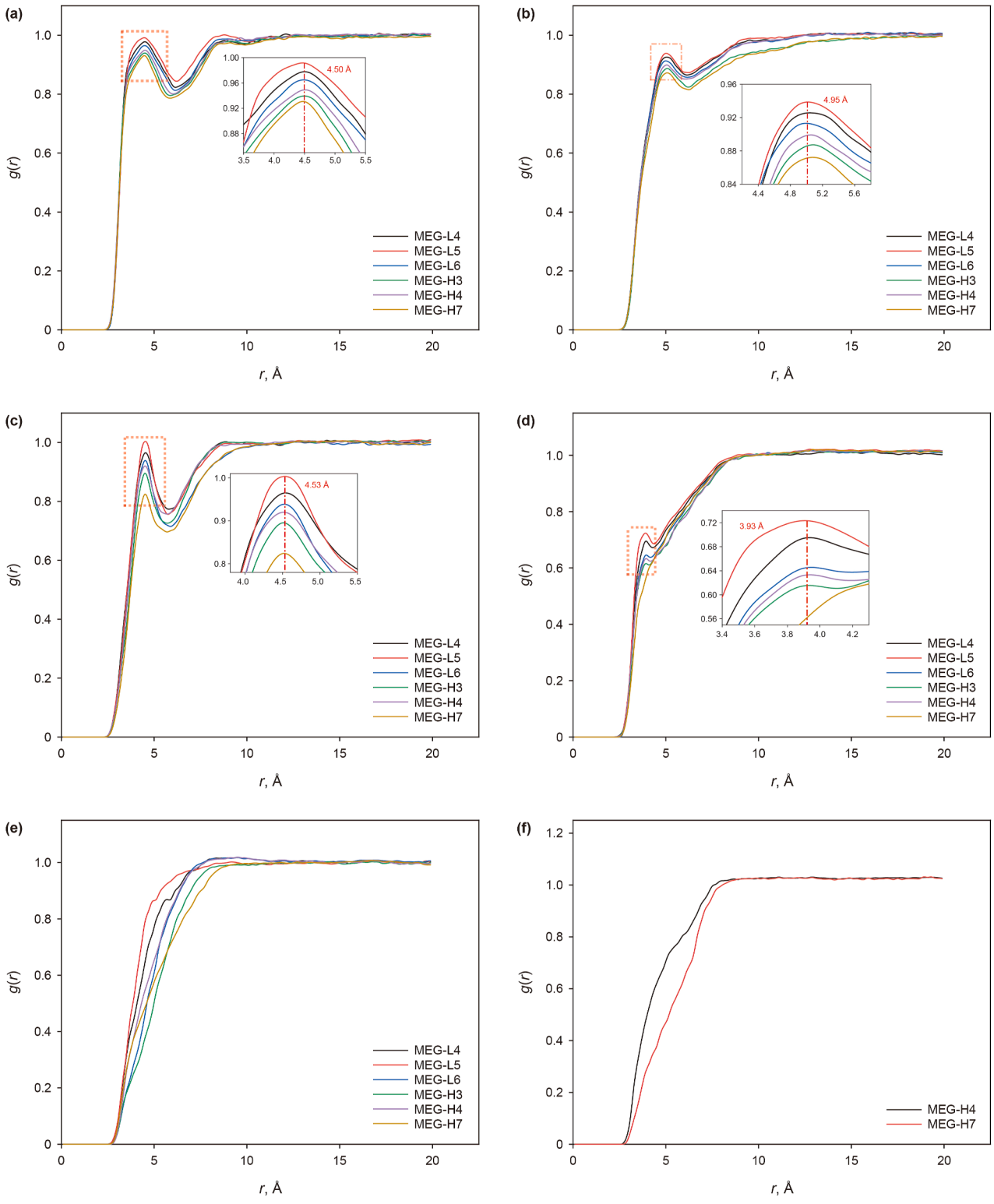

Fig. 14. RDFs between C atoms in MEG surfactants and O atoms in CO_2. (**a**) C_1–O in CO_2; (**b**) C_2–O in CO_2; (**c**) C_3–O in CO_2; (**d**) C_4–O in CO_2; (**e**) C_5–O in CO_2; (**f**) C_6–O in CO_2.

surfactants show stronger LA–LB interactions than cyclic ester surfactants. In contrast, C_5 and C_6 atoms, being sterically hindered, have limited CO_2 contact and contribute minimally to CO_2 affinity.

Fig. 15 shows RDFs of surfactant oxygen and hydrogen atoms with CO_2. CO_2 carbon and oxygen atoms aggregate around O_1 (carbonyl oxygen) at 3.26/3.42 Å and O_2 (ester ether oxygen) at 5.57/5.54 Å, following the trend MEG-L5 > MEG-L4 > MEG-L6 > MEG-H4 > MEG-H3 > MEG-H7. This shows that CO_2 aggregation around O_1/O_2 initially increases, then decreases with increasing ester group number. Cyclic multi-ester headgroup surfactants contain an additional ether oxygen O_3. CO_2 carbon and

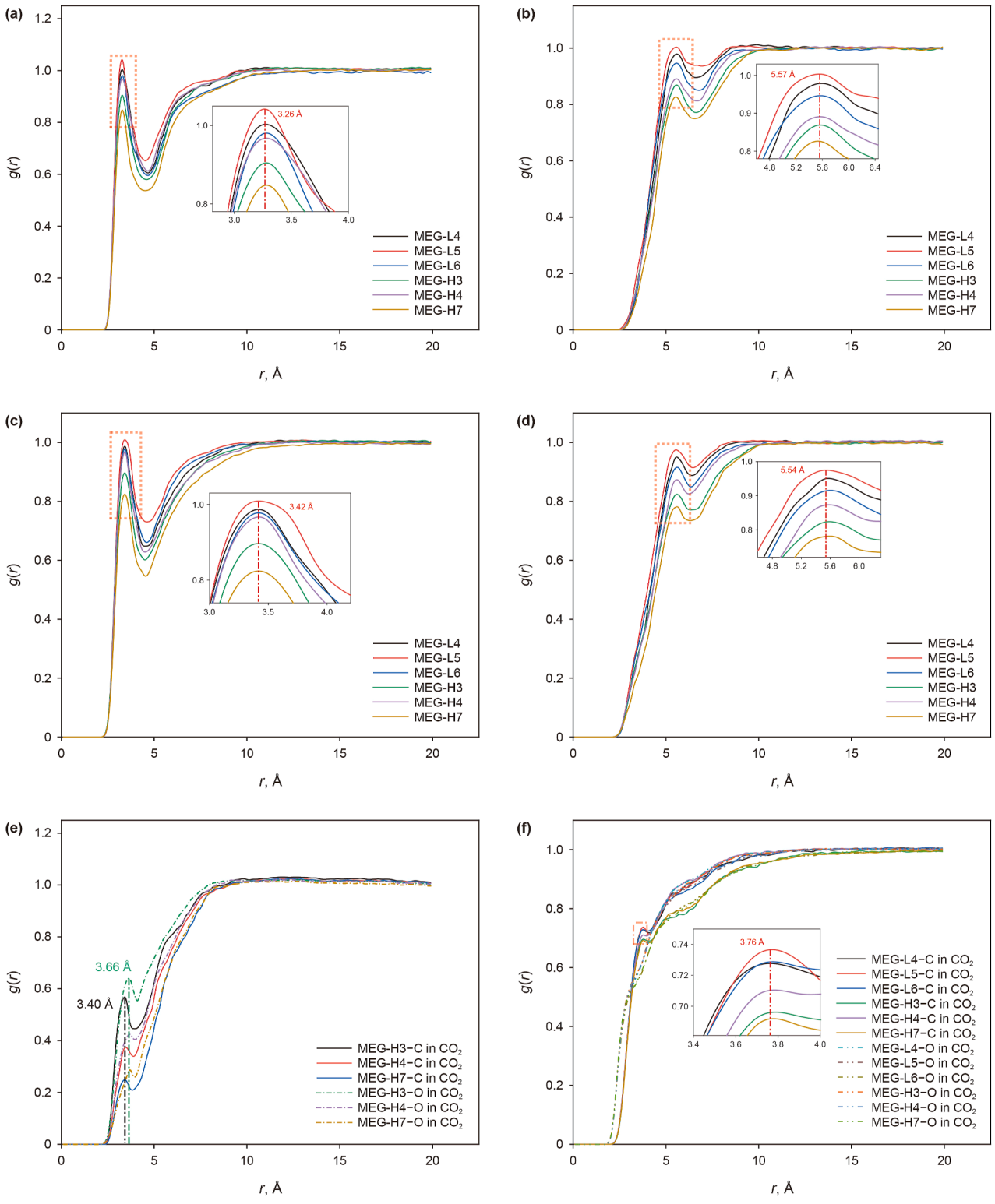

Fig. 15. RDFs between in MEG surfactants in CO_2. (**a**) O_1–C in CO_2; (**b**) O_2–C in CO_2; (**c**) O_1–O in CO_2; (**d**) O_2–O in CO_2; (**e**) O_3–CO_2; (**f**) H–CO_2.

oxygen atoms exhibit RDF peaks at 3.40 and 3.66 Å around O_3, indicating comparable LA–LB and dispersion interactions with CO_2. However, the O_3–O peak intensity exceeds that of O_3–C, suggesting that CO_2 oxygen atoms localize more readily around O_3 than CO_2 carbon atoms. For hydrogen atoms, an RDF peak at 3.76 Å with CO_2 carbon atoms suggests weak dispersion interactions with minimal contribution.

These findings support the following conclusions: (1) Linear ester surfactants are more effective than cyclic ester surfactants at promoting atomic-level dispersion and LA–LB interactions with

CO_2. (2) An optimal ester group number maximizes LA–LB and dispersion interactions. (3) Increasing ester group number introduces steric hindrance, limiting LA–LB and dispersion interactions.

3.4. Effect of spatial conformation on the solubility of multi-ester headgroup surfactants in CO_2

From an entropic perspective, higher mixing entropy enhances surfactant solubility in CO_2. Free volume and chain flexibility of surfactants strongly influence the entropy of the mixed system.

3.4.1. Effect of free volume fraction on CO_2 solubility

As CO_2 is a weak solvent, minor structural differences in solutes can lead to significant solubility variations, highlighting the critical role of surfactant free volume in solubility. Per the free volume theory by Fox and Flory, the macroscopic volume of a liquid or solid comprises occupied molecular volume and available free volume.

$$f_{free} = \frac{V_{free}}{V_{free} + V_{occupied}} \quad (5)$$

where f_{free} is the free volume fraction, %; V_{free} is the free volume, Å^3; and $V_{occupied}$ is the intrinsic volume of the molecule, Å^3.

Fig. 16 presents the variation in fractional free volume (FFV) calculated using the Connolly surface module. FFV reflects the available space for atomic motion within molecules. Higher FFV indicates greater conformational flexibility, promoting favorable conformations for effective CO_2 interactions, thus enhancing solubility. In single-component systems, linear ester headgroup surfactants exhibit significantly higher FFV than cyclic counterparts, suggesting greater flexibility and internal degrees of freedom in linear backbones. This enables linear surfactants to adopt conformations that interact effectively with CO_2. For linear multi-ester headgroup surfactants, FFV initially increases, then decreases with ester group number. At five ester groups, FFV peaks at 18.67%, indicating that CO_2-philic chain segments achieve maximum conformational mobility and form optimal CO_2-binding conformations. However, increasing ester group number further causes CO_2-philic chain entanglement, reducing free volume. In contrast, FFV of cyclic multi-ester headgroup surfactants decreases monotonically with increasing ester group number. Ester side chains, attached to a rigid cyclic backbone, exhibit restricted rotational flexibility. Although additional ester groups theoretically offer more binding sites (e.g., ester and methyl groups), the rigid backbone predominantly limits favorable conformation formation. Consequently, many potential binding sites fail to interact effectively with CO_2, reducing solubility.

Fig. 17 depicts the variation in FFV for surfactant–CO_2 binary systems. Lower FFV indicates tighter molecular packing and stronger surfactant–CO_2 interactions. For linear ester headgroup surfactants, FFV follows a decrease-then-increase trend with increasing ester group number, with MEG-L5 exhibiting the minimum FFV (50.44%). Initially, additional ester groups offer more CO_2 binding sites, enhancing solubility. Beyond the optimal number, inter-surfactant entanglement reduces available CO_2 binding sites, increasing FFV and decreasing solubility. For cyclic ester headgroup surfactants, FFV also decreases initially, then increases, with MEG-H4 (four ester groups) exhibiting the minimum FFV (51.08%). Unlike single-component systems, the cyclic backbone's rigidity counteracts the effect of additional ester groups, limiting CO_2-philic chain flexibility. In cyclic surfactants, ester group number and backbone rigidity compete: additional ester groups increase potential CO_2 interaction sites, while rigidity reduces conformational freedom and FFV, limiting solubility.

The design principles for surfactants with high CO_2 solubility are as follows: (1) Optimization of CO_2 binding sites: A moderate number of CO_2-philic groups, such as ester groups, ensures sufficient sites for effective CO_2 interactions. (2) Maintaining backbone flexibility: Excessively rigid or bulky backbones (e.g., cyclic structures) should be avoided, as they restrict conformational adaptability and hinder CO_2 binding. (3) Advantages of linear structures: Linear multi-ester headgroup surfactants exhibit high flexibility and large free volume, promoting favorable conformations for stable CO_2 binding. (4) Limitations of cyclic structures: Cyclic multi-ester headgroup surfactants, constrained by rigid backbones, show limited improvement in CO_2 solubility with additional ester groups, as steric hindrance reduces effective CO_2 binding.

3.4.2. Effect of chain segment variation on CO_2 solubility

Molecular simulation equilibrium results were used to analyze chain segment lengths in multi-ester headgroup surfactants, including: alkyl chains, CO_2-philic chains (in cyclic surfactants, the

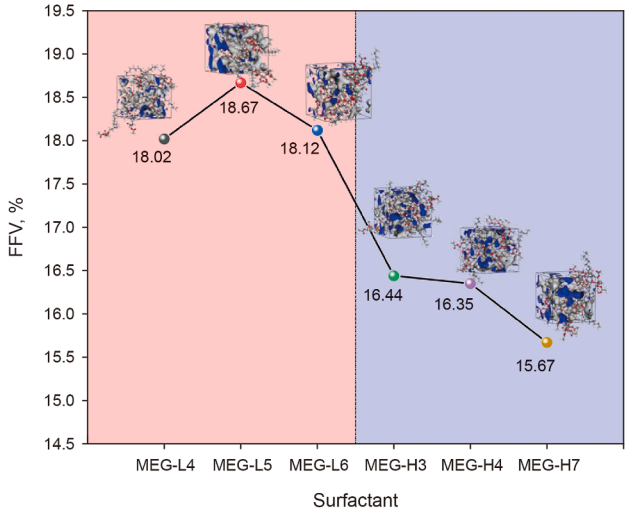

Fig. 16. FFV of multi-ester headgroup surfactants.

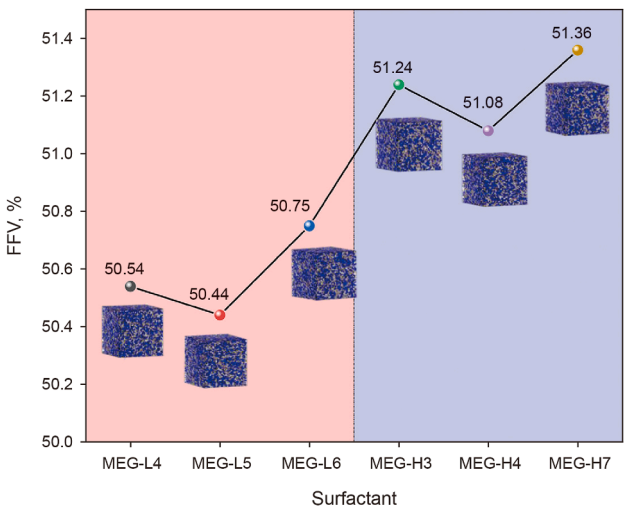

Fig. 17. FFV of MEG surfactant–CO_2 systems.

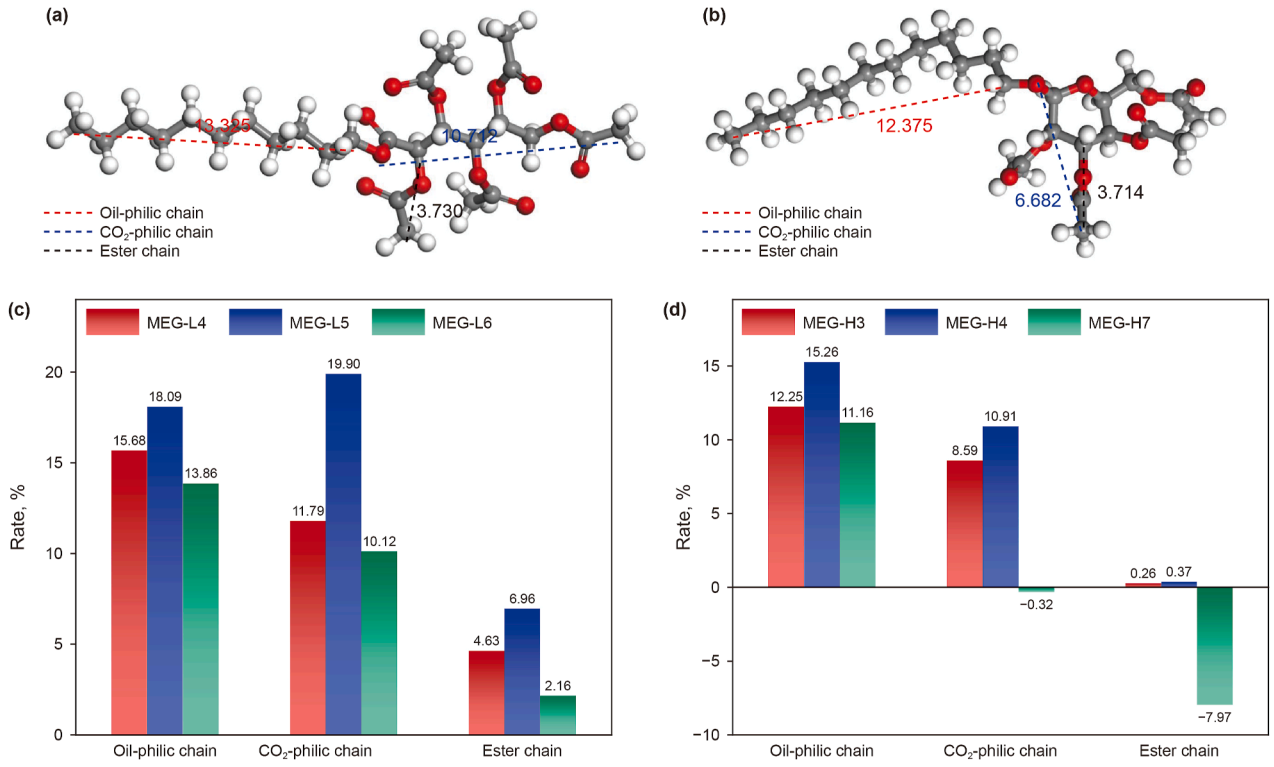

Fig. 18. Variations in the chain segments of MEG surfactants. Chain region segmentation of MGE-L4 (**a**) and MGE-H4 (**b**). Chain segment length variation rates for linear ester headgroup surfactants (**c**) and cyclic ester headgroup surfactants (**d**).

average length from distal ester chain ends to the cyclic backbone's starting point), and ester side chains (average length of all ester side chains).

$$Y = \frac{L_{sb} - L_{sa}}{L_{sb}} \times 100\% \quad (6)$$

where Y represents the percentage change in multi-ester headgroup surfactant chain segment length before and after equilibrium; L_{sb} denotes the segment length after equilibrium, Å; L_{sa} denotes the initial segment length, Å.

Fig. 18(a) and (b) depict chain region segmentation in linear and cyclic ester headgroup surfactants, respectively. At equilibrium, linear ester headgroup surfactants exhibit varying degrees of alkyl chains, with MEG-L5 exhibiting the greatest elongation (18.09%). CO_2-philic chains also extend significantly, with MEG-L5 showing the highest extension (19.9%). Ester side chains extend by over 2%, reaching 6.96% for MEG-L5. This suggests that increasing the number of ester groups enhances the density of CO_2-philic sites. The combined extension of CO_2-philic main chains and ester side chains maximizes surfactant–CO_2 contact. At six ester groups (MEG-L6), CO_2-philic chain extension decreases. Given that MEG-L6 exhibits the highest intermolecular interaction energy (Fig. 11(a)), this indicates intra- and intermolecular coiling, which reduces the number of effective CO_2 contact sites.

For cyclic ester headgroup surfactants, alkyl chains exhibit some extension. The CO_2-philic chain behavior varies: MEG-H3 and MEG-H4 extend, whereas MEG-H7 exhibits significant coiling (−0.32%). Ester side chains show minimal extension (<1%), with MEG-H7 shortening by −7.97%. These effects are attributed to the rigidity of the cyclic backbones. As the number of ester groups increases, the rotational flexibility of CO_2-philic chains decreases, sharply reducing the formation of favorable conformations and the entropy of mixing with CO_2. Although Potluri et al. (2003) suggested that outwardly extended, non-embedded cyclic CO_2-philic chains maximize CO_2 contact, the rigid backbone limits such conformations.

The following conclusions can be drawn: Linear multi-ester headgroup surfactants, owing to their greater backbone flexibility, enable cooperative deformation of the alkyl, CO_2-philic, and ester side chains. This promotes the formation of favorable conformations, thereby enhancing CO_2 contact sites as well as induced dipole and dispersion interactions. Cyclic multi-ester headgroup surfactants, despite having extended ester side chains, exhibit limited conformational adaptability due to backbone rigidity. This reduces effective CO_2 contact and weakens intermolecular interactions.

4. Conclusions

This study combines experimental investigations and molecular dynamics simulations to elucidate the dissolution behavior and mechanisms of multi-ester headgroup surfactants in supercritical CO_2. The key findings are as follows: Acetylation and esterification reactions enabled the successful synthesis of MEG surfactants with varying numbers and arrangements of ester group. MEG surfactants fully dissolve in CO_2 below 12 MPa, with linear ester headgroup surfactants showing superior solubility compared to cyclic structures. Among them, MEG-L5, which contains five linearly arranged ester groups, demonstrates the highest CO_2 solubility, with cloud point pressure of 9.32 MPa. This study proposes a microscopic mechanism for the dissolution of multi-ester headgroup surfactants in CO_2. CO_2 solubility is governed by both enthalpic and entropic contributions. From an enthalpic perspective, MEG–CO_2 intermolecular interactions are primarily driven by

van der Waals (vdW) and electrostatic forces, with vdW forces predominating. However, an excessive number of ester groups promotes surfactant self-aggregation, which reduces solubility. At the atomic level, the carbonyl oxygen and terminal methyl carbon in ester groups serve as primary CO_2 binding sites, with Lewis acid–base (LA–LB) and dispersion interactions synergistically enhancing CO_2 affinity. From an entropic perspective, free volume and chain flexibility are critical factors governing solubility. Linear structures, characterized by greater flexibility and larger free volume, more readily adopt favorable conformations for CO_2 interactions. Additionally, free volume and chain flexibility promote favorable enthalpic interactions. Design implications: Since that hydrocarbon-based surfactants interact with CO_2 primarily through LA–LB and dispersion forces, optimizing molecular chain architecture to maximize CO_2 binding sites and interactions is essential for enhancing solubility. The core design principle involves balancing the density of CO_2-philic groups and CO_2 accessibility to binding sites with molecular flexibility. This work provides a validated structure–performance framework for developing novel hydrocarbon-based CO_2-philic surfactants.

Furthermore, the multi-ester-headgroup design principle can be readily extended to other carbohydrate-based surfactants, such as sucrose esters and glucose esters. By systematically varying the number and spatial arrangement of ester groups, a diverse library of CO_2-philic surfactants can be developed, with potential applications not only in CO_2-enhanced oil recovery (EOR) but also in supercritical CO_2 extraction, foam-assisted geological CO_2 storage, and environmentally benign cleaning processes in the chemical industry. Nevertheless, translating these surfactants from laboratory to industrial scale faces several key challenges. Although the esterification route utilizes readily available renewable feedstocks, cost-effective large-scale production will require process optimization, such as adopting continuous-flow reactors or enzymatic catalysis, to compete with conventional CO_2-philic surfactants. Additionally, pilot-scale purification and quality control protocols remain to be validated. In contrast to persistent and potentially toxic fluorinated or siloxane-based surfactants, ester-based surfactants offer inherent biodegradability and are expected to undergo relatively rapid degradation in both subsurface reservoir and surface environments. These advantages are anticipated to unlock the full potential of multi-ester-headgroup CO_2-philic surfactants in CO_2-enhanced oil recovery and broader carbon utilization technologies.

CRediT authorship contribution statement

Ning Xu: Writing – review & editing, Writing – original draft, Supervision, Project administration, Methodology, Data curation. **Yan-Ling Wang:** Writing – review & editing, Supervision, Resources, Funding acquisition. **Baojun Bai:** Writing – review & editing, Validation, Supervision. **Shi-Zhang Cui:** Investigation, Funding acquisition. **Yu Zhang:** Methodology, Investigation. **Wen-Jing Shi:** Methodology, Investigation. **Zhao-Nian Zhang:** Methodology, Investigation. **Wen-Hui Ding:** Methodology, Investigation. **Pei-Xu Ma:** Methodology, Investigation. **Zan Gao:** Methodology, Investigation.

Declaration of competing interest

The authors declare that they have no known competing financial interests or personal relationships that could have appeared to influence the work reported in this paper.

Acknowledgements

We gratefully acknowledge the financial supports from the Key Technology Research and Development Program of Shandong (No. 2022CXGC020303) and the National Natural Science Foundation of China (Grant No. U22B6005).

Supplementary data

Supplementary data to this article can be found online at https://doi.org/10.1016/j.petsci.2026.06.010.

References

Altarsha, M., Ingrosso, F., Ruiz-Lopez, M.F., 2012. A new glimpse into the CO_2-philicity of carbonyl compounds. ChemPhysChem 13 (14), 3397–3403. https://doi.org/10.1002/cphc.201200135.

Alvarez, J.O., Schechter, D.S., 2017. Improving oil recovery in the Wolfcamp unconventional liquid reservoir using surfactants in completion fluids. J. Pet. Sci. Eng. 157, 806–815. https://doi.org/10.1016/j.petrol.2017.08.004.

Bao, L., Fang, S., Hu, D., et al., 2017. Enhancement of the CO_2-philicity of poly(vinyl ester)s by end-group modification with branched chains. J. Supercrit. Fluids 127, 129–136. https://doi.org/10.1016/j.supflu.2017.04.001.

Bray, C.L., Tan, B., Higgins, S., et al., 2010. Polymer CO_2 solubility. Structure/property relationships in polyester libraries. Macromolecules 43 (22), 9426–9433. https://doi.org/10.1021/ma1016055.

Criscenti, L.J., Cygan, R.T., 2013. Molecular simulations of carbon dioxide and water: Cation solvation. Environ. Sci. Technol. 47 (1), 87–94. https://doi.org/10.1021/es301608c.

Dai, J., Dong, D., Ni, Y., et al., 2024. Distribution patterns of tight sandstone gas and shale gas. Petrol. Explor. Dev. 51 (4), 767–779. https://doi.org/10.1016/S1876-3804(24)60505-7.

Dardin, A., DeSimone, J.M., Samulski, E.T., 1998. Fluorocarbons dissolved in supercritical carbon dioxide. NMR evidence for specific solute–solvent interactions. J. Phys. Chem. B 102 (10), 1775–1780. https://doi.org/10.1021/jp972127p.

Demirtas, C., Dilek, C., 2019. Enhanced solubility of siloxy-modified polyhedral oligomeric silsesquioxanes in supercritical carbon dioxide. J. Supercrit. Fluids 143, 358–364. https://doi.org/10.1016/j.supflu.2018.09.015.

DeSimone, J.M., Guan, Z., Elsbernd, C.S., 1992. Synthesis of fluoropolymers in supercritical carbon dioxide. Science 257 (5072), 945–947. https://doi.org/10.1126/science.257.5072.945.

Fan, X., Potluri, V.K., McLeod, M.C., et al., 2005. Oxygenated hydrocarbon ionic surfactants exhibit CO_2 solubility. J. Am. Chem. Soc. 127 (33), 11754–11762. https://doi.org/10.1021/ja052037v.

Gong, H., Lv, W., Zhang, H., et al., 2024. The influence and mechanism of alkyl block polyethers on the interfacial tension and minimum miscibility pressure of CO_2 and shale oil. Fuel 356, 129568. https://doi.org/10.1016/j.fuel.2023.129568.

Gong, H., Zhang, H., Lv, W., et al., 2025. Impact of citrate ester surfactants on the MMP, extraction and swelling behaviors between CO_2 and oil: Applications for enhanced shale oil recovery. Chem. Eng. Sci. 304, 121039. https://doi.org/10.1016/j.ces.2024.121039.

Greenhalgh, D.J., Williams, A.C., Timmins, P., et al., 1999. Solubility parameters as predictors of miscibility in solid dispersions. J. Pharmaceut. Sci. 88 (11), 1182–1190. https://doi.org/10.1021/js9900856.

Hansen, C.M., 1969. The universality of the solubility parameter. Prod. R&D 8 (1), 2–11. https://doi.org/10.1021/i360029a002.

Hildebrand, J.H., Scott, R.L., 1950. Solutions of nonelectrolytes. Annu. Rev. Phys. Chem. 1, 75–92. https://doi.org/10.1146/annurev.pc.01.100150.000451.

Hoefling, T.A., Enick, R.M., Beckman, E.J., 1991. Microemulsions in near-critical and supercritical carbon dioxide. J. Phys. Chem. 95 (19), 7127–7129. https://doi.org/10.1021/j100172a006.

Hu, D., Sun, S., Yuan, P., et al., 2015. Evaluation of CO_2-philicity of poly(vinyl acetate) and poly(vinyl acetate-*alt*-maleate) copolymers through molecular modeling and dissolution behavior measurement. J. Phys. Chem. B 119 (7), 3194–3204. https://doi.org/10.1021/jp5130052.

Inomata, H., Saito, S., Debenedetti, P.G., 1996. Molecular dynamics simulation of infinitely dilute solutions of benzene in supercritical CO_2. Fluid Phase Equilib. 116 (1–2), 282–288. https://doi.org/10.1016/0378-3812(95)02897-8.

Kazarian, S.G., Vincent, M.F., Bright, F.V., et al., 1996. Specific intermolecular interaction of carbon dioxide with polymers. J. Am. Chem. Soc. 118 (7), 1729–1736. https://doi.org/10.1021/ja950416q.

Kilic, S., Michalik, S., Wang, Y., et al., 2007. Phase behavior of oxygen-containing polymers in CO_2. Macromolecules 40 (4), 1332–1341. https://doi.org/10.1021/ma061422h.

Lee, J.J., Cummings, S.D., Beckman, E.J., et al., 2017. The solubility of low molecular weight poly(dimethyl siloxane) in dense CO_2 and its use as a CO_2-philic

segment. J. Supercrit. Fluids 119, 17–25. https://doi.org/10.1016/j.supflu.2016.08.003.
Lemaire, P., Beckman, E., Enick, R., 2022. Mixtures of CO_2 and poly(fluoroacrylate) based on monomers containing only six or four fluorinated carbons: Phase behavior and solution viscosity. J. Supercrit. Fluids 190, 105728. https://doi.org/10.1016/j.supflu.2022.105728.
Li, S., Dang, F., Du, K., et al., 2026. Dissolution behavior of multiester surfactants in CO_2Potentially for carbon geological storage: Experimental measurements and molecular dynamics simulations. Langmuir 42 (1), 675–690. https://doi.org/10.1021/acs.langmuir.5c04800.
Liao, P., Liu, Z., Liu, K., et al., 2020. Polyesters-based oil-CO_2 amphiphiles: Design and miscible promoting ability. Acta Phys. Chim. Sin. 36 (10), 1907034. https://doi.org/10.3866/PKU.WHXB201907034 (in Chinese).
Liu, B., Shi, J., Sun, B., et al., 2015. Molecular dynamics simulation on volume swelling of CO_2–alkane system. Fuel 143, 194–201. https://doi.org/10.1016/j.fuel.2014.11.046.
Liu, J., Han, B., Li, G., et al., 2001. Solubility of the non-ionic surfactant tetraethylene glycol *n*-laurel ether in supercritical CO_2 with n-pentanol. Fluid Phase Equilib. 187–188, 247–254. https://doi.org/10.1016/s0378-3812(01)00539-8.
Liu, J., Han, B., Wang, Z., et al., 2002a. Solubility of Ls-36 and Ls-45 surfactants in supercritical CO_2 and loading water in the CO_2/water/surfactant systems. Langmuir 18 (8), 3086–3089. https://doi.org/10.1021/la011721u.
Liu, J., Han, B., Zhang, J., et al., 2002b. Formation of water-in-CO_2 microemulsions with non-fluorous surfactant Ls-54 and solubilization of biomacromolecules. Chem. Eur J. 8 (6), 1356–1360. https://doi.org/10.1002/1521-3765(20020315)8:6<1356::AID-CHEM1356>3.0.CO;2-N.
Lv, W., Gong, H., Li, Y., et al., 2020. Dissolution behaviors of alkyl block polyethers in CO_2: Experimental measurements and molecular dynamics simulations. Chem. Eng. Sci. 228, 115953. https://doi.org/10.1016/j.ces.2020.115953.
Lv, W., Gong, H., Li, Y., et al., 2022. The potential and mechanism of nonionic polyether surfactants dissolved in CO_2 to improve the miscibility of CO_2–hydrocarbon systems. Fuel 326, 125012. https://doi.org/10.1016/j.fuel.2022.125012.
Lv, W., Dong, M., Sarma, H., et al., 2023. Effects of CO_2-philic nonionic polyether surfactants on miscibility behaviors of CO_2–hydrocarbon systems: Experimental and simulation approach. Chem. Eng. J. 464, 142701. https://doi.org/10.1016/j.cej.2023.142701.
Ma, C., Dou, X., Liu, Z., et al., 2022. Application and mechanism of a novel CO_2-oil miscible flooding agent, CAA8-X. Acta Phys. Chim. Sin. 38 (8), 2012019. https://doi.org/10.3866/PKU.WHXB202012019. (in Chinese).
Ma, S.L., Wu, Y.T., Hurrey, M.L., et al., 2010. Sugar acetates as CO_2-philes: Molecular interactions and structure aspects from absorption measurement using quartz crystal microbalance. J. Phys. Chem. B 114 (11), 3809–3817. https://doi.org/10.1021/jp9122634.
Mohamed, A., Ardyani, T., Sagisaka, M., et al., 2015. Economical and efficient hybrid surfactant with low fluorine content for the stabilisation of water-in-CO_2 microemulsions. J. Supercrit. Fluids 98, 127–136. https://doi.org/10.1016/j.supflu.2015.01.012.
Neises, B., Steglich, W., 1978. Simple method for the esterification of carboxylic acids. Angew. Chem. Int. Ed. 17 (7), 522–524. https://doi.org/10.1002/anie.197805221.
Potluri, V.K., Xu, J., Enick, R., et al., 2002. Peracetylated sugar derivatives show high solubility in liquid and supercritical carbon dioxide. Org. Lett. 4 (14), 2333–2335. https://doi.org/10.1021/ol026007y.
Potluri, V.K., Hamilton, A.D., Karanikas, C.F., et al., 2003. The high CO_2-solubility of per-acetylated α-, β-, and γ-cyclodextrin. Fluid Phase Equilib. 211 (2), 211–217. https://doi.org/10.1016/S0378-3812(03)00206-1.
Raveendran, P., Wallen, S.L., 2002. Cooperative C–H···O hydrogen bonding in CO_2–Lewis base complexes: Implications for solvation in supercritical CO_2. J. Am. Chem. Soc. 124 (42), 12590–12599. https://doi.org/10.1021/ja0174635.
Rigby, D., Sun, H., Eichinger, B.E., 1997. Computer simulations of poly(ethylene oxide): Force field, PVT diagram and cyclization behaviour. Polym. Int. 44 (3), 311–330. https://doi.org/10.1002/(SICI)1097-0126(199711)44:3<311::AID-PI880>3.0.CO;2-H.
Sarbu, T., Styranec, T., Beckman, E.J., 2000. Non-fluorous polymers with very high solubility in supercritical CO_2 down to low pressures. Nature 405 (6783), 165–168. https://doi.org/10.1038/35012040.
Shi, Q., Qiao, W., 2017. Synthesis of siloxane polyether surfactants and their solubility in supercritical CO_2. J. Surfactants Deterg. 20 (2), 453–458. https://doi.org/10.1007/s11743-016-1912-x.
Small, P.A., 1953. Some factors affecting the solubility of polymers. J. Appl. Chem. 3 (2), 71–80. https://doi.org/10.1002/jctb.5010030205.
Standnes, D.C., Nogaret, L.A.D., Chen, H.L., et al., 2002. An evaluation of spontaneous imbibition of water into oil-wet carbonate reservoir cores using a nonionic and a cationic surfactant. Energy Fuels 16 (6), 1557–1564. https://doi.org/10.1021/ef0201127.
Sukee, A., Nunta, T., Fongkham, N., et al., 2022a. Effects of brine valency and concentration on oil displacement by spontaneous imbibition: An interplay between wettability alteration and reduction in the oil-brine interfacial tension. J. Mol. Liq. 365, 120089. https://doi.org/10.1016/j.molliq.2022.120089.
Sukee, A., Nunta, T., Haruna, M.A., et al., 2022b. Influence of sequential changes in the crude oil-water interfacial tension on spontaneous imbibition in oil-wet sandstone. J. Petrol. Sci. Eng. 210, 110032. https://doi.org/10.1016/j.petrol.2021.110032.
Temtem, M., Casimiro, T., Santos, A.G., et al., 2007. Molecular interactions and CO_2-philicity in supercritical CO_2. A high-pressure NMR and molecular modeling study of a perfluorinated polymer in scCO_2. J. Phys. Chem. B 111 (6), 1318–1326. https://doi.org/10.1021/jp0660233.
Thompson, A.P., Aktulga, H.M., Berger, R., et al., 2022. LAMMPS - a flexible simulation tool for particle-based materials modeling at the atomic, meso, and continuum scales. Comput. Phys. Commun. 271, 108171. https://doi.org/10.1016/j.cpc.2021.108171.
Wang, M., Fang, T., Wang, P., et al., 2016. The self-assembly structure and the CO_2-philicity of a hybrid surfactant in supercritical CO_2: Effects of hydrocarbon chain length. Soft Matter 12 (39), 8177–8185. https://doi.org/10.1039/c6sm01584k.
Xie, X., Weiss, W.W., Tong, Z., et al., 2005. Improved oil recovery from carbonate reservoirs by chemical stimulation available. SPE J. 10 (3), 276–285. https://doi.org/10.2118/89424-PA.
Xu, N., Wang, Y., Bai, B., et al., 2025. Dissolution mechanism of nonionic polyether surfactants in supercritical CO_2. Energy Fuels 39 (33), 15601–15621. https://doi.org/10.1021/acs.energyfuels.5c02127.
Yang, J., Ren, Y., Tian, A.M., et al., 2000. COMPASS force field for 14 inorganic molecules, He, Ne, Ar, Kr, Xe, H_2, O_2, N_2, NO, CO, CO_2, NO_2, CS_2, and SO_2, in liquid phases. J. Phys. Chem. B 104 (20), 4951–4957. https://doi.org/10.1021/jp992913p.
Yee, G.G., Fulton, J.L., Smith, R.D., 1992. Fourier transform infrared spectroscopy of molecular interactions of heptafluoro-1-butanol or 1-butanol in supercritical carbon dioxide and supercritical ethane. J. Phys. Chem. 96 (15), 6172–6181. https://doi.org/10.1021/j100194a017.
Zhang, C., Xi, L., Wu, P., et al., 2020. A novel system for reducing CO_2-crude oil minimum miscibility pressure with CO_2-soluble surfactants. Fuel 281, 118690. https://doi.org/10.1016/j.fuel.2020.118690.
Zhang, H., Gong, H., Wu, J., et al., 2024a. Promoting dissolution behaviors of low-carbon alcohol polyoxyethylene polyoxypropylene ether in CO_2 by molecular structure optimization and adding cosolvent. J. Mol. Liq. 406, 125115. https://doi.org/10.1016/j.molliq.2024.125115.
Zhang, J., Pan, Z., Liu, K., et al., 2013. Molecular simulation of CO_2 solubility and its effect on octane swelling. Energy Fuels 27 (5), 2741–2747. https://doi.org/10.1021/ef400283n.
Zhang, W., Guo, P., Jia, N., et al., 2024b. The effects of nonionic surfactants on enhancing miscibility between oil and CO_2: A molecular dynamics study. J. Mol. Liq. 408, 125076. https://doi.org/10.1016/j.molliq.2024.125076.
Zhang, X., Zhang, T., Ge, J., et al., 2021. The CO_2-in-water foam stabilized with the mixture of CO_2-soluble surfactant and nonionic surfactant. J. Pet. Sci. Eng. 198, 108117. https://doi.org/10.1016/j.petrol.2020.108117.
Zhao, L., Lin, S., Mendenhall, J.D., et al., 2011. Molecular dynamics investigation of the various atomic force contributions to the interfacial tension at the supercritical CO_2–water interface. J. Phys. Chem. B 115 (19), 6076–6087. https://doi.org/10.1021/jp201190g.
Zhao, L., Tao, L., Lin, S., 2015. Molecular dynamics characterizations of the supercritical CO_2–mediated hexane–brine interface. Ind. Eng. Chem. Res. 54 (9), 2489–2496. https://doi.org/10.1021/ie505048c.